haematologica
Journal of the Ferrata Storti Foundation

Increased RhoA pathway activation downstream of αIIbβ3/SRC contributes to heterozygous Bernard Soulier syndrome

by Larissa Lordier, Christian A. Di Buduo, Alexandre Kauskot, Nathalie Balayn, Cécile Lavenu-Bombled, Francesco Baschieri, Valérie Proulle, Cecilia P. Marin Oyarzun, Francesca Careddu, Ida Biunno, Tudor Manoliu, Philippe Rameau, Isabelle Plo, Nicolas Papadopoulos, Stefan Constantinescu, William Vainchenker, Guillaume Nam Nguyen, Paola Ballerini, Remi Favier, Alessandra Balduini and Hana Raslova

Received: August 9, 2024.
Accepted: February 28, 2025.

Citation: Larissa Lordier, Christian A. Di Buduo, Alexandre Kauskot, Nathalie Balayn, Cécile Lavenu-Bombled, Francesco Baschieri, Valérie Proulle, Cecilia P. Marin Oyarzun, Francesca Careddu, Ida Biunno, Tudor Manoliu, Philippe Rameau, Isabelle Plo, Nicolas Papadopoulos, Stefan Constantinescu, William Vainchenker, Guillaume Nam Nguyen, Paola Ballerini, Remi Favier, Alessandra Balduini and Hana Raslova. Increased RhoA pathway activation downstream of αIIbβ3/SRC contributes to heterozygous Bernard Soulier syndrome.
Haematologica. 2025 Mar 6. doi: 10.3324/haematol.2024.286424 [Epub ahead of print]

Increased RhoA pathway activation downstream of αIIbβ3/SRC contributes to heterozygous Bernard Soulier syndrome

Larissa Lordier[1,2,3,4*], Christian A. Di Buduo[5*], Alexandre Kauskot[6], Nathalie Balayn[2,3,4], Cécile Lavenu-Bombled[7], Francesco Baschieri[8], Valérie Proulle[9,10], Cecilia P. Marin Oyarzun[2,3,4], Francesca Careddu[5], Ida Biunno[11], Tudor Manoliu[4,12], Philippe Rameau[4,12], Isabelle Plo[2,3,4], Nicolas Papadopoulos[13,14], Stefan Constantinescu[13,14,15,16], William Vainchenker[2,3,4], Guillaume Nam Nguyen[17], Paola Ballerini[17], Remi Favier[17], Alessandra Balduini[5,18], Hana Raslova[2,3,4#]

[*]Equal contribution

[1] INOVARION, Paris, France
[2] INSERM, UMR1287, Gustave Roussy, Villejuif, France, Equipe labellisée Ligue Nationale Contre le Cancer
[3] Université Paris-Saclay, UMR 1287, Gustave Roussy, Villejuif, France
[4] Gustave Roussy, UMR 1287, Villejuif, France
[5] Department of Molecular Medicine, University of Pavia, Pavia, Italy.
[6] INSERM U1176, Hemostasis, Inflammation & Thrombosis (HITh), Université Paris-Saclay, Le Kremlin-Bicêtre, France.
[7] Paris Saclay University, INSERM U1176 (HITh), AP-HP, Hematology Department, Bicêtre Hospital, Le Kremlin-Bicêtre, France
[8] Institute of Pathophysiology, Biocenter, Medical University of Innsbruck, Innsbruck, Austria.
[9] Service Hématologie Biologique, Hôpital Cochin, AP-HP.Centre - Université Paris Cité, France
[10] Unite INSERM UMRS 1138, CRC, France
[11] Integrated Systems Engineering, Bresso-Milano, Italy.
[12] UMS AMMICa 23/3655, Plateforme Imagerie et Cytométrie, Gustave Roussy, Université Paris-Saclay, Villejuif, France
[13] Ludwig Institute for Cancer Research, Brussels, Belgium
[14] Université Catholique de Louvain and de Duve Institute, SIGN Unit, Brussels, Belgium
[15] Walloon Excellence in Life Sciences and Biotechnology, Brussels, Belgium
[16] Ludwig Institute for Cancer Research, Nuffield Department of Medicine, Oxford University, Oxford, United Kingdom
[17] Assistance Publique-Hôpitaux de Paris, Hôpital Armand Trousseau, Centre de Référence des pathologies plaquettaires, Paris, France.
[18] Department of Biomedical Engineering, Tufts University, Medford, United States.

[#] **Corresponding author:** Hana RASLOVA PhD**,** INSERM UMR1287, Gustave Roussy, 114 rue Edouard Vaillant, 94805 Villejuif, France, E-mail: Hana.Raslova@gustaveroussy.fr, Phone: (+33) 1 42 11 46 71

Running head: "RhoA activation contributes to heterozygous BSS"

Acknowledgments
The authors thank the patients for participation in this study, Pr. M.C. Alessi who coordinates the "Centre de Référence des pathologies plaquettaires" (France); Sylvie Souquere from Electronic microscopy platform, UMS3655-AMMICA, Gustave Roussy Villejuif, France and Cyril Catelain from the Imaging and Cytometry Core Facility (PFIC) (Unit AMMICa, Gustave Roussy) for their expertise and advices in using instruments and methodological developments.
Dr. Carolina P. Miguel, Dr. Matteo Migliavacca for technical assistance with confocal microscopy; Dr. Marco Lunghi for technical assistance with CAD design and 3D printing, 'Centro Grandi Strumenti' of the University of Pavia, Italy.

Funding
The work was supported by H2020-FETOPEN-1-2016-2017- SilkFusion (n. 767309) and EIC Transition project SilkPlatelet (n. 101058349) to A. Balduini and H. Raslova and by ANR-22-CE17-0043-01 MacroIT to H. Raslova.

Author Contributions
LL, CADB, AK, NB, FB, CPMO, FC, IB, NP, TM, PR performed and analyzed experiments. CLB; VP, PB, RF provided patient samples. LL, CADB, AK, FB, IB, TM, PR, CLB; VP, PB, RF, IP, NP, SC, WV, AB, HR discussed results. HR supervised the work. LL, CADB, VW, IP, AB and HR wrote the article. LL and CADB equally contributed to this work. All the authors contributed to the final approval of the manuscript.

Conflict of interest disclosures
The authors declare no competing financial interests.

Data sharing statement: Data generated in this study are available within this paper and upon request from the corresponding author. Any additional information required to reanalyze the data reported in this study is available from the corresponding author upon request.

ABSTRACT

Bernard Soulier Syndrome (BSS) is a severe bleeding disorder with moderate to severe thrombocytopenia, giant platelets, and platelet dysfunction, caused by biallelic mutations in *GP1BA*, *GP1BB*, or *GP9* genes. We generated induced pluripotent stem cells (iPSC) from a BSS patient with a novel heterozygous *GP1BA* p.N103D mutation, resulting in moderate macrothrombocytopenia. The mutation does not affect megakaryocyte (MK) differentiation or GPIb-GPIX complex expression but reduces affinity to von Willebrand factor (VWF). It induces increased signaling independent of VWF and αIIbβ3-mediated outside-in signaling, causing a profound defect in proplatelet formation after adhesion on fibrinogen. Pre-activation of αIIbβ3 integrin and heightened stress fiber formation linked to RhoA pathway overactivation were observed, likely due to increased phosphorylation of SRC at Y419 downstream of GPIbα. Dasatinib, a SRC inhibitor, restored stress fiber formation. Using a 3D bone marrow model to mimic platelet release under flow, we demonstrated that the ROCK1/2 inhibitor Y27632 increased platelet number and restored platelet size in GPIbα N103D MKs, as well as in MKs from two other patients with heterozygous *GP1BA* mutations (p.L160P and p.N150S). However, Y27632 had no additional effect on platelet generation from MKs of two patients with biallelic BSS, suggesting a distinct molecular mechanism in biallelic cases.

INTRODUCTION

Bernard Soulier Syndrome (BSS; MIM #231200) is an autosomal recessive disorder due to quantitative or qualitative defects of the GPIb-IX complex with a severe bleeding diathesis. Presently, more than 50 missense, nonsense or frameshift mutations have been reported in *GP1BA*, *GP1BB* or *GP9* genes coding for GPIbα, GPIbβ and GPIX, while no defect has been found in the GP5 gene, coding for the GPV subunit.[1] BSS is characterized by moderate to severe thrombocytopenia, giant platelets, and platelet dysfunction, and has an estimated incidence of 1/1,000,000. Although it was reported that giant platelets could be related to defects in proplatelet formation (PPF) from patient megakaryocytes (MKs), the precise mechanisms leading to macrothrombocytopenia are unknown.

A few cases with autosomal dominant transmission (monoallelic BSS) and mild bleeding have also been described. *GP1BA*^{A156V} (or p.A172V) also called Bolzano mutation is the most frequent heterozygous mutation.[2,3]

The role of glycoprotein GPIb-IX complex in platelet functions is well established. Its interaction with von Willebrand Factor (VWF) plays a major role in platelet adhesion and plug formation at sites of vascular injury. However, its involvement in regulating platelet production remains poorly understood. The use of *Gp1ba* and *Gp1bb* KO mice revealed a role of this receptor during the final stages of MK maturation, notably the formation of the DMS and proplatelet extension[4,5], likely independently of VWF since *Vwf* KO mice display no MKpoiesis defect.[6] Similarly, human MKs derived from induced pluripotent stem cells (iPSC) of homozygous BSS patients carrying mutations in *GP1BA* or *GP1BB,* did not express the GPIb-GPIX complex on their cell surface. This led to the production of abnormally large proplatelets and macroplatelet-like particles with a dilated demarcation membrane system (DMS)[7], mirroring the findings in mice.

In platelets, it is well established that VWF binding to the GPIb-IX complex initiates platelet activation turning on several signaling pathways such as Src family kinases (Lyn and Src), SYK, Rac1, PI3-kinase/Akt, BAD, cGMP-dependent protein kinase and MAP kinases.[8-10] Indeed, the interaction of the intracytoplasmic domain of GPIbα with 14-3-3ζ, after VWF binding, initiates a signaling cascade leading to integrin αIIbβ3 activation.[11] However, less is known about GPIb-GPIX-mediated signaling in the MK lineage. It has been shown that the absence of the cytoplasmic tail of GPIbα prevents 14-3-3ζ interaction and phosphorylation of AKT, which could impair thrombopoietin-mediated responses.[12] However, this does not explain the defect in DMS and the presence of macrothrombocytopenia in BSS. The

interaction between GPIbα with cytoskeleton proteins and mainly with Filamin A (FLNa) was proposed as regulator of platelet formation and size in mouse models[5,13-15] but only a slight effect on *in vitro* PPF was detected in the absence of GPIbα/FLNa interaction in human MKs derived from iPSCs induced from patients with Filaminopathy A[16], suggesting that other mechanisms could be involved.

In heterozygous BSS, the Bolzano Ala156Val mutation was shown to reduce PPF by half.[17] However, the mechanism by which mutations in the extracellular domain of GPIbα, while maintaining intracellular interactions, lead to such a defect, has not been explored. Here, we derived iPSCs from a BSS patient with a novel heterozygous mutation in the extracellular leucine-rich repeats (LLR) domain of *GP1BA*^{N103D}, resulting in mild macrothrombocytopenia. We report an overactivation in the RhoA pathway due to increased SRC phosphorylation. Employing a 3D bone marrow model to simulate platelet release under flow conditions[18,19], we demonstrate that ROCK1/2 inhibition restores platelet number and size for heterozygous BSS patients with mutations in the extracellular LRR domain of *GP1BA* but not for homozygous BSS patients with a homozygous mutation in the extracellular LRR domain of *GP1BA* or *GP1BB.*

METHODS

Study approval

Blood samples from patients and healthy subjects were collected after informed written consent and obtained in accordance with the Declaration of Helsinki. The study was approved by the Comité de Protection des Personnes CPP N°2020T2-02, France.

Five unrelated individuals (P1-P5) were identified with macrothrombocytopenia during routine blood tests (**ST1**).

iPSCs generation and expansion

$CD34^+$ cells obtained from peripheral blood of P1 patient were cultured in a serum-free medium supplemented with cytokines for 6 days and transduced using the CytoTune iPS 2.0 Sendai Reprogramming Kit (Thermo Fisher).

Flow Cytometry

Single cell suspensions were subjected to staining using monoclonal antibodies directly coupled to their respective fluorochromes. Analysis was conducted using BD Canto II or BD LSRFortessa cytometers (BD Biosciences). MKs were isolated on Influx, ARIA III, or ARIA Fusion cell sorters (BD Biosciences).

Silk bone marrow model

Silk fibroin aqueous solution was obtained from *B. mori* silkworm cocoons according to previously published literature.[20] Silk scaffolds have been produced by a salt-leaching method, as previously described.[21] The dynamic perfusion of the 3D silk bone marrow model was performed by using a peristaltic pump (ShenChen Flow Rates Peristaltic Pump - LabV1) connected to a bioreactor chamber manufactured using 3D SLA printing technology (Form 3B (Formlab)) and consisted of two wells each of which was equipped with a 3D silk fibroin scaffold. 1.5×10^5 MKs were seeded into each silk scaffold and kept at 37 °C and 5% CO_2.

Statistics

All data are shown as mean±SEM, mean±SD or mean±min to max. The statistical analyses were performed using the PRISM software. Statistical significance was established using a Student's *t* test or a One Way Analysis of Variance (ANOVA) specified in legends. Differences were considered significant at $P < 0.05$.

RESULTS

To investigate the mechanism of macrothrombocytopenia in patients with monoallelic *GP1BA* mutation, we derived iPSCs from a female patient with mild macrothrombocytopenia (P1, $118x10^9$ platelets/L) and rare hemorrhagic manifestations such as epistaxis and ecchymosis. The patient exhibited a slight defect in platelet aggregation (70-80% response to ADP, EPI, COL, AA, TRAP and ristocetin) and carried a new heterozygous p.N103D mutation in the extracellular LLR4 domain of the *GP1BA* gene that was initially identified by NGS and confirmed by Sanger sequencing (**SF1, ST1**). For these reasons, the patient was classified as monoallelic Bernard Soulier Syndrome. Three different clones were characterized and utilized for subsequent studies (**SF2**). Additionally, three previously described independent iPSC lines were employed as controls.[22-24]

GPIbα^{N103D} expression in megakaryocytes

MKs were differentiated from iPSCs using a previously described protocol.[16] The cell surface expression levels of αIIb (CD41), GPIX (CD42a), and GPIbα (CD42b) in MKs were unaffected by the presence of the *GP1BA*^{N103D} mutation (**Figure 1A**), as well as their total cellular level as shown by Western blot analysis (**Figure 1B, SF 3A**). In computational modeling, the 3D structure of the GPIbα^{N103D} mutant remained unaffected (**Figure 1C**). Immunological staining of MKs showed no difference in GPIbα distribution (**Figure 1D, SF 3B**).

Normal maturation of GPIbα^{N103D} megakaryocytes

GPIbα^{N103D} did not affect the ploidy level (**SF 3C**). Electronic microscopy revealed no defect in maturation with normal DMS and α-granule formation (**SF 3D**), as also attested by the immunostaining of GPIbα, actin (**Figure 1D**) and VWF (**SF 3E**). A slight increase in actin distribution on the cell membrane was detected (**SF 3B**). GPIbα has been proposed to regulate DMS and PPF formation through its interaction with the cytoskeleton, particularly Filamin A. However, Filamin distribution was similar to that observed in control MKs (**Figure 1D, SF 3B)**, and the co-immunoprecipitation assay performed with anti-GPIbα antibody revealed no defect in the interaction between GPIbα and FLNa (**Figure 1E**). A trend towards reduced MK activation in response to thrombin was observed, with a significant decrease at 0.5 U/mL, as indicated by the membrane expression of P-selectin (**Figure 1F**).

Abnormal proplatelet formation by GPIbα^{N103D} megakaryocytes

We then investigated proplatelet formation by mutant versus control MKs in a liquid culture containing thrombopoietin (TPO) and stem cell factor (SCF). No difference in the percentage of proplatelet-forming MKs was detected (**Figure 2A**). The analysis of proplatelets revealed an increased size of tips with a slight decrease in the distribution of GPIbα on the tips and decreased GPIbα level at the surface of platelet-like particles generated *in vitro* (**SF 4A, B, C**). This is consistent with a slight increase in GPIbα shedding during proplatelet formation (SF 4D). After adhesion on fibrinogen (20 µg/mL) for 72 hours, a 2.5-fold decrease in the percentage of MKs forming proplatelets was detected (**Figure 2B**).

To accurately assess the differences in both quantity and size of platelets produced by mutant and control samples, $CD41^{+}CD42^{+}$ mature MKs were introduced into a 3D bone marrow model made of silk fibroin and functionalized with 50 µg/mL fibrinogen. The system was perfused for 6 hours with culture medium to collect platelets, which were then quantified using flow cytometry (**Figure 2C**). Platelet diameters were measured after adhesion on polylysine-coated slides using Arivis Vision 4D (Zeiss). Compared to controls, 3.35 times fewer platelets were recovered from GPIbα^{N103D} MKs (**Figure 2D**), and their size was significantly larger (**Figure 2E**), confirming that MKs derived from patient-specific iPSCs replicate the characteristics of BSS. The increased size of platelets was also confirmed by electron microscopy (**Figure 2F**). A 1.57-fold reduction in platelet numbers was also

observed when the 3D bone marrow model was functionalized with 50 µg/mL fibronectin (**SF 4D, E**). Interestingly, only a slight increase in platelet size was detected (**SF 4D, F**) suggesting that the macrothrombocytopenia depends primarily on fibrinogen activation on αIIbβ3.

Decreased VWF binding in the presence of GPIbα^{N103D} mutant

To understand how the GPIbα^{N103D} mutant affects receptor function and platelet aggregation, we first investigated the adhesion of MKs on VWF. The adhesion of $CD41^{+}CD42^{+}$ MKs on VWF for 30 min was not affected (**SF 5A**). However, when cells were incubated with ristocetin (0.5 mg/mL) and different concentrations of soluble VWF for 30 min, decreased sensitivity was detected by flow cytometry in the presence of a low dose (0.1 µg/mL of VWF) (**SF 5B**). The specificity of the binding of VWF (0.1 µg/mL) to the GPIb complex was confirmed after incubation with a blocking anti-CD42b antibody (**SF 5C**). These results show that like other BSS monoallelic mutations that are not predicted to bind VWF[25], GPIbα p.N103D decreases the affinity of the GPIbα-GPIX receptor for VWF.

Increased RhoA activation in GPIbα^{N103D} megakaryocytes

Next, we assessed whether the GPIbα^{N103D} mutant could affect αIIbβ3-mediated signaling in MKs. We examined the activation of αIIbβ3 under basal conditions and after activation with thrombin. In the basal state, integrins predominantly exist in an inactive state on the cell surface until they receive an external signal. In basal condition, incubation of MKs with the PAC1 antibody, directed against the active αIIbβ3 conformation, or with fibrinogen-FITC showed no significant difference in PAC1 and fibrinogen binding between GPIbα^{N103D} mutant and control MKs, respectively (**SF 6A, B, Figure 3A**). To investigate whether the GPIbα^{N103D} mutant could induce increased pre-activation of the αIIbβ3 complex, MKs were activated with thrombin (1U/mL) for 5 minutes and then incubated either with PAC-1 or with fibrinogen-FITC. As depicted in **Figure 3A**, a slight but significant increase in fibrinogen binding was detected for the mutated MKs after activation with thrombin and a similar tendency was detected for PAC-1 (**SF 6A, C**). To confirm that the GPIbα^{N103D} mutant induces unusual αIIbβ3 activation, MKs were plated onto a fibrinogen matrix for 30 minutes, and cell morphology was analyzed by fluorescence microscopy after labeling the F-actin network. GPIbα^{N103D} led to an increased spreading with a higher percentage of MKs forming stress fibers (56.4% for mutant MKs versus 22.4% for control MKs) (**Figure 3B**). This increased

stress fiber formation was not observed after adhesion onto fibronectin and VWF. This suggests that although no increased αIIbβ3 activation was detected by flow cytometry under basal conditions, the GPIbα^{N103D} mutant may prime αIIbβ3 for activation in the absence of VWF. Interestingly, thrombin stimulation significantly increased the percentage of stress fiber-forming MKs in the control group, rising from 20.3% to 50.6%, which matched the frequency of spread MKs observed in GPIbα^{N103D} mutant MKs without stimulation (**SF 6D**). The effect was even more pronounced in GPIbα^{N103D} mutant MKs, where the percentage increased from 41.6% to 81.6%.

Stress fiber formation being a hallmark of RhoA activation, we further focused on RhoA pathway. Using a lentiviral FRET biosensor based on the Raichu probe[16], we measured RhoA activity. A slight but significant increase in RhoA activity was detected in GPIbα^{N103D} MKs after adhesion to fibrinogen compared to controls (**Figure 3C**). This finding matches with the mild macrothrombocytopenia induced by this mutant. Previously, it was demonstrated that the GPIb-GPIX complex regulates the balance between RhoA and CDC42 signaling.[26] Therefore, we also measured CDC42 activity under the same conditions and observed a slight decrease in CDC42 activity (**Figure 3C**), confirming that the GPIbα^{N103D} mutant deregulates the RhoA/CDC42 balance.

Inhibition of RhoA pathway restores stress fiber formation, platelet production and platelet size

The main RhoA effector that regulates acto-myosin cytoskeleton reorganization through Myosin Light Chain 2 (MLC2) phosphorylation in MKs is the Rho-associated kinase (ROCK). To assess its overactivation in GPIbα^{N103D} MKs, we first investigated the localization of P-MLC2 and demonstrated its colocalization with F-actin during abnormal stress fiber formation after adhesion to fibrinogen (**SF 7A**). Notably, treatment of MKs with the Y27632 ROCK1/2 inhibitor resulted in a 3.9-fold decrease in the proportion of stress fiber-forming MKs (**Figure 3D, E**) after adhesion to fibrinogen for 30 minutes.

ROCK1/2 inhibition increased the percentage of proplatelet-forming GPIbα^{N103D} MKs after adhesion to fibrinogen to a level close to normal MKs (**Figure 3F, SF 7B**). To precisely quantify the impact of ROCK1/2 inhibition on platelet production and platelet size, MKs were seeded in the 3D silk bone marrow model functionalized with fibrinogen and incubated or not with Y27632. This niche mimic was housed into a perfusable chamber. The flow through the scaffold enabled platelets to detach and release into the perfused culture medium, with or

without Y27632. Platelets were collected into a collection bag, and their number was estimated using flow cytometry with counting beads. Incubation with Y72632 led to a 2.2-fold increase in the platelet count generated by GPIbα^{N103D} MKs, a level close to normal MKs with a partial correction of platelet size (**Figure 3G, H, SF 7C**). 1.4-fold increase in the platelet number was also detected for normal MKs.

GPIbα^{N103D} mutant induces increased P-SRC Y419 and P-STAT3 Y705 levels, and accelerates microtubules kinetics

How GPIb precisely regulates the RhoA pathway in MKs remains unclear. The GPIbα is linked through its cytoplasmic domain to proteins necessary for the DMS formation, such as PACSIN2 and FLNa.[15] Additionally, its interaction with the adaptor protein 14-3-3ζ activates a signaling cascade leading to αIIbβ3 activation in platelets. The GPIbα^{N103D} mutation does not affect FLNa interaction and DMS formation. To gain further insights into the mechanism by which this mutant could activate the RhoA pathway, we performed a phosphoproteome analysis on MKs after adhesion to fibrinogen. Two independent experiments revealed increased phosphorylation of different proteins, including SRC at tyrosine Y419 and STAT3 on tyrosine Y705 and serine S727 (**Figure 4A, SF 8**). SRC has been reported to activate GEF-H1 either directly or indirectly through STAT3 phosphorylation at tyrosine Y705, both leading to the release GEF-H1 from microtubules and allowing RhoA activation.[27-29] Hence, we confirmed increased phosphorylation of STAT3 at Y705 and SRC at Y419 by Western blot (**Figure 4B**). Finally, when phosphorylation of SRC was inhibited using a non-specific SRC inhibitor dasatinib (**Figure 4C**), a 2.14-fold decrease in the frequency of stress fiber-forming MKs was detected (**Figure 4D, E**).

RhoA inhibition restores platelet production from heterozygous but not homozygous BSS

To confirm the implication of the RhoA pathway in heterozygous BSS, we examined the effect of the ROCK1/2 inhibitor Y27632 on *in vitro*-derived megakaryopoiesis and platelet generation in two patients carrying *GP1BA*^{L160P} (P2) and *GP1BA*^{N150S} (P3) mutations in LRR6, respectively. MK differentiation (**Figure 5A, 6A**) and the expression of αIIb (CD41) and the GPIb-GPIX complex (CD42) at the cell surface (**Figure 5B, 6B**) were not affected. On day 10 of culture CD41^{+}CD42^{+} MKs were sorted, seeded into the 3D bioreactor (**Figure 5C, SF 9**), and perfused into the flow chamber to collect platelets. A 2.12-fold increase in

platelet yield was detected for P2, compared to a 1.48-fold increase for control platelets after incubation with the ROCK1/2 inhibitor (**Figure 5D**).

The inhibition of the RhoA pathway led to a 1.3-fold decrease in platelet size for P2 and a 1.19-fold decrease for control platelets (CNT2) (**Figure 5E**). For P3, the ploidy was also examined without detecting any defect (**Figure 6C**), and a 4.67-fold increase in platelet number was observed compared to a 1.48-fold increase for control platelets (CNT) (**Figure 6D**). The inhibition of the RhoA pathway led to a 1.32-fold decrease in platelet size for P3 while no decrease was detected for control platelets (CNT3) (**Figure 6E**). Overall, these results demonstrate that the inhibition of the RhoA pathway in heterozygous BSS partially restores the generation of normal-sized platelets. The effect of RhoA inhibition is more significant in the patients' samples than in controls, where RhoA is still activated but to a lesser degree, and thus its inhibition has a less pronounced effect on platelet generation.

Finally, we examined the effect of RhoA inhibition on homozygous BSS patients carrying homozygous *GP1BB*^{G43W} (P4) and *GP1BA*^{L139P} (P5) mutations, respectively. No defect in the frequency of MKs was detected (**SF 10A, E**). However, while αIIb (CD41) expression at the cell surface of MKs was normal, a substantial decrease in GPIb-GPIX complex (CD42) expression was observed for both patients (**SF 10B, F**). The modal ploidy level, measured only for P4, was also considerably decreased (N=6.9 for control MKs versus N=3.35 for patient MKs) (**SF 10C**). A decreased frequency of proplatelet-forming MKs was detected for P4, with no specific effect of RhoA inhibition, as shown by a 1.4-fold increase for control MKs and a 1.38-fold increase for patient MKs (**SF 10D**). For P5, the effect of RhoA inhibition on platelet production was evaluated in the 3D culture system, as for P2 and P3 (**SF 10G-I**). The number of platelets generated by an identical number of MKs was decreased, but no specific effect of RhoA inhibition was evidenced (**SF 10H**). The inhibition of the RhoA pathway led to only a 1.15-fold decrease in platelet size for P5 while no decrease was detected for control platelets (CNT) (**SF 10I**). These results indicate that RhoA inhibition does not restore platelet generation, suggesting, together with decreased ploidy for P4, that the mechanism of thrombocytopenia in homozygous BSS is not the same as in heterozygous BSS.

DISCUSSION

In this study we have developed an iPSC-based model of monoallelic BSS that demonstrates 1) the mechanism by which heterozygous *GP1BA* mutations lead to a defect in platelet production by activating the RhoA pathway, 2) that by using a 3D bone marrow model we

can detect the rescue of platelet formation and size from MKs with heterozygous BSS, but not from homozygous BSS, under treatment with a ROCK1/2 inhibitor.

We report the first iPSC monoallelic BSS model derived from a patient with a new heterozygous mutation in the LRR4 domain of GPIbα, *GP1BA*^{N103D}. This mutation does not affect the expression of the GPIb-GPIX complex, DMS formation and GPIbα/FLNa interaction in contrast to previously described BSS models that rely on homozygous deletions in mice[4,5,30] or homozygous mutations in *GP1BB* and *GP1BA* in iPSC models[7], leading to the absence or a profound decrease in GPIb complex expression at the cell surface and defects in DMS development. These findings suggest a different mechanism as in homozygous BSS, leading only to mild macrothrombocytopenia.

The abrogation of the GPIb-VWF interaction was demonstrated to affect proplatelet formation under shear, emphasizing the contribution of the extracellular domain of GPIb.[31] However, IL-4R/GPIbα-Tg mice, with an extracellular IL-4 receptor and an intracellular GPIbα cytoplasmic tail, partially restored platelet formation and platelet size compared to GPIbα-deficient mice[13], suggesting that both intracellular and extracellular GPIbα domains are important for platelet generation.

This led us to hypothesize that point mutations in the extracellular domain of GPIbα and conserved intracellular domain in monoallelic BSS will affect inside-out signaling to αIIbβ3. A profound defect in PPF after adhesion on fibrinogen and increased stress fiber formation suggested an enhanced activation of the fibrinogen receptor αIIbβ3 and an overactivation of the RhoA pathway. Despite the absence of increased PAC-1 and fibrinogen binding at the steady state, their increased binding after activation by thrombin confirmed an increased αIIbβ3 pre-activation in the presence of the GPIb mutant. The enhanced RhoA activation after the adhesion of mutant MKs on fibrinogen was probably due to increased signaling mediated by αIIbβ3. It is now well established that RhoA should be partially inactivated at the end of MK maturation to ensure normal thrombopoiesis[32], and that GPIb controls a RhoA/CDC42 balance in this process[26], which is clearly deregulated in the presence of the GPIbα^{N103D} mutant. As a result, the treatment of MKs with a ROCK1/2 inhibitor not only decreased stress fiber formation but also restored PPF. Utilizing the recently described 3D silk-based bone marrow model,[18,19] which provides a favorable niche for thrombopoiesis, and includes a flow-through system that mimics the bloodstream to enable platelet release and collection, we demonstrated that treatment with a ROCK1/2 inhibitor not only restores the number of platelets generated but also their size.

In agreement with the basal RhoA activation, a slight effect of the ROCK1/2 inhibitor was also observed on healthy MKs but was less pronounced than in mutant MKs. Excessive acto-myosin contractility due to the overactivation of RhoA or its effectors leads to macrothrombocytopenia in MYH-9 syndrome[33] and in Filaminopathy A.[16] Under normal conditions, FLNa maintains RhoA in an inactive state, and in its absence, RhoA becomes activated. However, in GPIbα^{N103D} MKs, FLNa is normally localized, and no defect in the GPIbα-FLNa interaction is detected, suggesting that the mechanism of RhoA activation is different.

The cytoplasmic domain of GPIbα also interacts with the signal transduction molecule 14-3-3ζ[11], which mediates the phosphorylation of many substrates in platelets. In MKs, disruption of this interaction was shown to increase P-AKT levels, ploidization, and proliferation of MKs.[12] However, the domain necessary for the interaction between GPIbα and 14-3-3ζ is conserved in the GPIbα^{N103D} mutant. Thus, to better understand the mechanism, proteomic arrays were performed and revealed increased phosphorylation in some proteins, including SRC at tyrosine Y419, which caught our attention. Indeed, SRC belongs to the Src family kinases that are associated with or in close proximity to αIIbβ3 and GPIb-GPIX receptors, transmitting signals to downstream effectors. Alongside Fyn and Lyn, SRC was shown to be implicated in the early stages of VWF-GPIb-GPIX mediated inside-out signaling to αIIbβ3 in platelets.[34,35] Through its direct interaction with the β3 subunit of αIIbβ3 integrin, SRC could also be involved in outside-in signaling after binding to fibrinogen.[36] Although VWF binding is required for GPIbα-mediated inside-out signaling in platelets, the GPIb-mediated signaling in MKs is poorly understood. The affinity of VWF is decreased in the presence of GPIbα^{N103D} mutant, and this could lead to a defect in platelet release under shear[31] and thus participate to thrombocytopenia. However, no thrombocytopenia is observed in *vwf* KO mice[6], and defects in platelet generation were observed in the absence of VWF, suggesting that the increased signaling is directly linked to the *GP1BA*^{N103D} mutation. The precise mechanism remains to be understood, but one of the explanations would be the induction of GPIb-GPIX receptor clustering leading to increased signaling to αIIbβ3 in the absence of vWF. Indeed, GPIb-GPIX clustering has been shown to increase adhesive function of αIIbβ3 after exposition to immobilized fibrinogen.[37]

Whether the increased phosphorylation of SRC on Y419 is directly mediated by mutant GPIbα^{N103D}, or indirectly as a consequence of GPIbα^{N103D}-induced pre-activation of αIIbβ3, or both, remains to be understood. Interestingly, SRC was shown to activate GEF-H1, the exchange factor involved in RhoA activation in MKs[38], by its release from microtubules.

GEF-H1 activation could be mediated by SRC either directly [27] or indirectly through SRC-mediated phosphorylation of STAT3 on tyrosine Y705.[39,40,28,29] Therefore, the overactivation of RhoA could be a consequence of increased P-SRC Y419 downstream of GPIbα^{N103D}. According to this hypothesis, the SRC inhibitor Dasatinib decreases stress fiber formation, however further studies are necessary to confirm GEF-H1 activation in presence of GPIbα mutant.

Finally, the 3D-silk-based model was employed to closely replicate the bone marrow structure and perfusion, allowing us to validate the restoration of platelet generation and size following ROCK1/2 inhibition for two other monoallelic BSS patients with *GP1BA* p.L160P and p.N150S mutations. Notably, the application of Y27632 had no additional impact on platelet generation from MKs derived from two patients with biallelic BSS, as compared to control.

In conclusion, our findings indicate that monoallelic BSS is, at least in part, attributed to a defect in the late stages of megakaryopoiesis. This defect arises from dysregulated GPIbα-mediated VWF- independent signaling to αIIbβ3, leading to increased αIIbβ3 pre-activation, and increased SRC phosphorylation and RhoA activation after fibrinogen binding. In contrast, biallelic BSS involves different mechanisms, more closely aligning with the phenotype observed in *Gp1ba* and *Gp1bb* knockout mice, which is characterized by a defect in DMS.

References

1. Savoia A, Kunishima S, De Rocco D, et al. Spectrum of the mutations in Bernard-Soulier syndrome. Hum Mutat. 2014;35(9):1033-1045.
2. Ware J, Russell SR, Marchese P, et al. Point mutation in a leucine-rich repeat of platelet glycoprotein Ib alpha resulting in the Bernard-Soulier syndrome. J Clin Invest. 1993;92(3):1213-1220.
3. Noris P, Perrotta S, Bottega R, et al. Clinical and laboratory features of 103 patients from 42 Italian families with inherited thrombocytopenia derived from the monoallelic Ala156Val mutation of GPIbα (Bolzano mutation). Haematologica. 2012;97(1):82-88.
4. Poujol C, Ware J, Nieswandt B, Nurden AT, Nurden P. Absence of GPIbalpha is responsible for aberrant membrane development during megakaryocyte maturation: ultrastructural study using a transgenic model. Exp Hematol. 2002;30(4):352-360.
5. Strassel C, Eckly A, Léon C, et al. Intrinsic impaired proplatelet formation and microtubule coil assembly of megakaryocytes in a mouse model of Bernard-Soulier syndrome. Haematologica. 2009;94(6):800-810.
6. Denis C, Methia N, Frenette PS, et al. A mouse model of severe von Willebrand disease: defects in hemostasis and thrombosis. Proc Natl Acad Sci U S A. 1998;95(16):9524-9529.
7. Mekchay P, Ingrungruanglert P, Suphapeetiporn K, et al. Study of Bernard-Soulier Syndrome Megakaryocytes and Platelets Using Patient-Derived Induced Pluripotent Stem Cells. Thromb Haemost. 2019;119(9):1461-1470.
8. Aitken A. 14-3-3 and its possible role in co-ordinating multiple signalling pathways. Trends Cell Biol. 1996;6(9):341-347.
9. Muslin AJ, Tanner JW, Allen PM, Shaw AS. Interaction of 14-3-3 with signaling proteins is mediated by the recognition of phosphoserine. Cell. 1996;84(6):889-897.
10. Zha J, Harada H, Yang E, Jockel J, Korsmeyer SJ. Serine phosphorylation of death agonist BAD in response to survival factor results in binding to 14-3-3 not BCL-X(L). Cell. 1996;87(4):619-628.
11. Mangin PH, Receveur N, Wurtz V, David T, Gachet C, Lanza F. Identification of five novel 14-3-3 isoforms interacting with the GPIb-IX complex in platelets. J Thromb Haemost. 2009;7(9):1550-1555.
12. Kanaji T, Russell S, Cunningham J, Izuhara K, Fox JE, Ware J. Megakaryocyte proliferation and ploidy regulated by the cytoplasmic tail of glycoprotein Ibalpha. Blood. 2004;104(10):3161-3168.
13. Kanaji T, Russell S, Ware J. Amelioration of the macrothrombocytopenia associated with the murine Bernard-Soulier syndrome. Blood. 2002;100(6):2102-2107.
14. Jurak Begonja A, Hoffmeister KM, Hartwig JH, Falet H. FlnA-null megakaryocytes prematurely release large and fragile platelets that circulate poorly. Blood. 2011;118(8):2285-2295.
15. Begonja AJ, Pluthero FG, Suphamungmee W, et al. FlnA binding to PACSIN2 F-BAR domain regulates membrane tubulation in megakaryocytes and platelets. Blood. 2015;126(1):80-88.
16. Donada A, Balayn N, Sliwa D, et al. Disrupted filamin A/α(IIb)β(3) interaction induces macrothrombocytopenia by increasing RhoA activity. Blood. 2019;133(16):1778-1788.
17. Balduini A, Malara A, Pecci A, et al. Proplatelet formation in heterozygous Bernard-Soulier syndrome type Bolzano. J Thromb Haemost. 2009;7(3):478-484.
18. Di Buduo CA, Wray LS, Tozzi L, et al. Programmable 3D silk bone marrow niche for platelet generation ex vivo and modeling of megakaryopoiesis pathologies. Blood. 2015;125(14):2254-2264.

19. Di Buduo CA, Laurent PA, Zaninetti C, et al. Miniaturized 3D bone marrow tissue model to assess response to Thrombopoietin-receptor agonists in patients. Elife. 2021;10:e58775.
20. Rockwood DN, Preda RC, Yücel T, Wang X, Lovett ML, Kaplan DL. Materials fabrication from Bombyx mori silk fibroin. Nat Protoc. 2011;6(10):1612-1631.
21. Di Buduo CA, Soprano PM, Tozzi L, et al. Modular flow chamber for engineering bone marrow architecture and function. Biomaterials. 2017;146:60-71.
22. Secardin L, Gomez Limia C, da Silva-Benedito S, et al. Induced Pluripotent Stem Cells Enable Disease Modeling and Drug Screening in Calreticulin del52 and ins5 Myeloproliferative Neoplasms. Hemasphere. 2021;5(7):e593.
23. Saliba J, Hamidi S, Lenglet G, et al. Heterozygous and homozygous JAK2(V617F) states modeled by induced pluripotent stem cells from myeloproliferative neoplasm patients. PLoS One. 2013;8(9):e74257.
24. Antony-Debré I, Manchev VT, Balayn N, et al. Level of RUNX1 activity is critical for leukemic predisposition but not for thrombocytopenia. Blood. 2015;125(6):930-940.
25. Uff S, Clemetson JM, Harrison T, Clemetson KJ, Emsley J. Crystal structure of the platelet glycoprotein Ib(alpha) N-terminal domain reveals an unmasking mechanism for receptor activation. J Biol Chem. 2002;277(38):35657-35663.
26. Dütting S, Gaits-Iacovoni F, Stegner D, et al. A Cdc42/RhoA regulatory circuit downstream of glycoprotein Ib guides transendothelial platelet biogenesis. Nat Commun. 2017;8:15838.
27. Azoitei ML, Noh J, Marston DJ, et al. Spatiotemporal dynamics of GEF-H1 activation controlled by microtubule- and Src-mediated pathways. J Cell Biol. 2019;218(9):3077-3097.
28. Pan YR, Chen CC, Chan YT, et al. STAT3-coordinated migration facilitates the dissemination of diffuse large B-cell lymphomas. Nat Commun. 2018;9(1):3696.
29. Joo E, Olson MF. Regulation and functions of the RhoA regulatory guanine nucleotide exchange factor GEF-H1. Small GTPases. 2021;12(5-6):358-371.
30. Ware J, Russell S, Ruggeri ZM. Generation and rescue of a murine model of platelet dysfunction: the Bernard-Soulier syndrome. Proc Natl Acad Sci U S A. 2000;97(6):2803-2808.
31. Dunois-Lardé C, Capron C, Fichelson S, Bauer T, Cramer-Bordé E, Baruch D. Exposure of human megakaryocytes to high shear rates accelerates platelet production. Blood. 2009;114(9):1875-1883.
32. Chang Y, Auradé F, Larbret F, et al. Proplatelet formation is regulated by the Rho/ROCK pathway. Blood. 2007;109(10):4229-4236.
33. Chen Y, Boukour S, Milloud R, et al. The abnormal proplatelet formation in MYH9-related macrothrombocytopenia results from an increased actomyosin contractility and is rescued by myosin IIA inhibition. J Thromb Haemost. 2013;11(12):2163-2175.
34. Senis YA, Mazharian A, Mori J. Src family kinases: at the forefront of platelet activation. Blood. 2014;124(13):2013-2024.
35. Wu Y, Asazuma N, Satoh K, et al. Interaction between von Willebrand factor and glycoprotein Ib activates Src kinase in human platelets: role of phosphoinositide 3-kinase. Blood. 2003;101(9):3469-3476.
36. Shattil SJ, Kim C, Ginsberg MH. The final steps of integrin activation: the end game. Nat Rev Mol Cell Biol. 2010;11(4):288-300.
37. Kasirer-Friede A, Ware J, Leng L, et al. Lateral clustering of platelet GP Ib-IX complexes leads to up-regulation of the adhesive function of integrin alpha IIbbeta 3. J Biol Chem. 2002;277(14):11949-11956.
38. Gao Y, Smith E, Ker E, et al. Role of RhoA-specific guanine exchange factors in regulation of endomitosis in megakaryocytes. Dev Cell. 2012;22(3):573-584.

39. Laird AD, Li G, Moss KG, et al. Src family kinase activity is required for signal tranducer and activator of transcription 3 and focal adhesion kinase phosphorylation and vascular endothelial growth factor signaling in vivo and for anchorage-dependent and -independent growth of human tumor cells. Mol Cancer Ther. 2003;2(5):461-469.
40. Garcia R, Bowman TL, Niu G, et al. Constitutive activation of Stat3 by the Src and JAK tyrosine kinases participates in growth regulation of human breast carcinoma cells. Oncogene. 2001;20(20):2499-2513.

LEGENDS

Figure 1. GPIbα^{N103D} mutant does not affect megakaryocyte differentiation from iPSC.
A. Flow cytometry plots showing expression of CD41, CD42a and CD42b on control (CNT1, CNT2) and GPIba^{N103D} (2 different clones were used) megakaryocytes (MKs). **B**. Representative western blot of GPIb-GPIX complex (GPIbα, GPIbβ, GPIX) on mature control (CNT) and GPIba^{N103D} MKs. GAPDH, HSC70 and Actin were used as loading controls. Quantification is shown in SF 3A. **C.** 3D structure predicted by using AlphaFold Protein Structure Database (https://alphafold.ebi.ac.uk/entry/P07359). hGPIbα Wild-type and hGPIbα N103D mutants aligned, focus on N/D103. **D,** Representative immunofluorescence staining pictures of mature control (CNT) an GPIbα^{N103D} MKs: GPIbα (CD42b, green), F-actin (gray), Filamin A (red), DAPI (nuclei, blue). Scale bar: 2 μm, z-stack middle frame is shown. **E.** Co-immunoprecipitation assay performed on control (CNT) and GPIbα^{N103D} MKs confirming the interaction between GPIbα and Filamin A (FNLa). Mouse anti-GPIbα was used for immunoprecipitation and both anti-GPIbα and rabbit anti-FLNa antibodies were used for Western blot assay. The quantification revealed no defect in the GPIbα-FLNa interaction in presence of GPIbα^{N103D} mutant. **F.** Flow cytometry analysis of P-selectin at cell surface after activation of MKs with indicated concentration of Thrombin for 5 min. Anti-P-selectin antibody conjugated with PE was used. Data represent the mean±SEM, n=3, **P*<0.05, paired t-test.

Figure 2. GPIbα^{N103D} mutant alters proplatelet formation and platelet generation.
A. Frequency of proplatelet forming control (CNT) and GPIbα^{N103D} mutant MKs cultured in liquid medium in presence of TPO and SCF. Data are expressed as mean±SEM (CNT n=7, GPIbα^{N103D} n=10). **B.** Frequency of proplatelet forming control (CNT) and GPIbα^{N103D} mutant MKs on after adhesion of slides coated with 20 μg/mL of fibrinogen. Data are expressed as mean±SEM (CNT n=6, GPIbα^{N103D} n=3), ****P*<0.001, unpaired t-test. **C.** Schematic representation of *ex vivo* platelet collection from MKs cultured into the silk bone marrow model functionalized with fibrinogen (50 μg/mL). 1.5x10^5 control (CNT) and GPIbα^{N103D} mutant MKs were seeded into scaffolds. Samples were perfused with culture medium, into a multi-well flow chamber, for 6 hours. Released platelets were collected into gas-permeable bags. Samples were mixed with counting beads to quantify the number of platelets that were identified as CD41$^+$CD42a$^+$ events. **D.** The number of recovered platelets is shown. Data are expressed as mean±SEM (CNT n=3, GPIba^{N103D} n=3), **P*<0.05, unpaired t-test. **E.** Platelet diameters (μm) of *ex vivo*-released platelets were measured by Arivis Vision 4D (Zeiss). Data are expressed as mean±min to max, CNT: n=127, GPIbα^{N103D}: n=136, *****P*<0.0001, unpaired t-test. **F.** Transmission electron microscopy of *ex vivo* produced platelets (scale bar: 2μm).

Figure 3. GPIbα^{N103D} mutant induces an increase in RhoA activity downstream αIIbβ3.
A. Flow cytometry analysis Fibrinogen (Fb) binding to αIIbβ3 receptor on control (CNT) and GPIbα^{N103D} mutant MKs before and after its activation by Thrombin (Thr). MKs were stimulated or not for 5 minutes with Thrombin (1U/mL) and then incubated with Alexa 488-conjugated Fibrinogen. Representative picture of plots is shown on the left panel. The histogram presenting the Mean Fluorescence Intensity (MFI) of Fibrinogen (Fb) staining at basal state is shown on the middle panel and after stimulation by Thrombin on the right panel. The MFI after stimulation was normalized to the corresponding condition without stimulation. The histograms present the MFI of Fb normalized to 1 control in each experiment. Three independent experiments are shown. Data are expressed as mean±SEM (CNT n=5,

GPIba^{N103D} n=5). *P<0.05, Mann-Whitney test. **B.** Spreading assay of mature control (CNT) and GPIbα^{N103D} mutant MKs plated on different substrates. Representative picture of immunofluorescence staining of MKs plated on fibrinogen-coated surface and stained for F-actin (green) and DAPI (blue) is shown on the left panel, single z-stack frame at the glass adhesion site is shown. The histogram presenting the frequency (%) of stress fiber forming MKs plated on fibrinogen-, VWF- or fibronectin-coated surface is shown on the right panel. Data are expressed as mean±SEM, n=4, **P<0.01, paired t-test. **C.** FRET analysis for RhoA or Cdc42 activation on fibrinogen-coated surface. At least 15 cells per condition were analyzed in each experiment. The histograms represent the average of 4-5 independent experiments. Data are normalized to control condition (CNT) for each experiment and are expressed in arbitrary units (a.u.) as mean±SEM, n=5 for RhoA, n=4 for CDC42, **P<0.01, Mann-Whitney test. **D-E.** Immunofluorescence analysis of stress fibers formation by mature control (CNT) and GPIbα^{N103D} mutant MKs. Mature MKs were plated on fibrinogen-coated surface in presence or absence of ROCK1/2 inhibitor Y27632 for 30 min and stained for F-Actin (green) and DAPI (blue). **D.** Representative pictures of immunofluorescence staining. Scale bar: 30µm, single z-stack frame at the glass adhesion site is shown. **E.** The histogram presenting the frequency (%) of stress fiber forming MKs plated on fibrinogen-coated surface. Data are expressed as mean±SEM, n=4, *P<0.05, **P<0.01, One Way Analysis of Variance (ANOVA) with Tukey's multiple comparison method was used. **F.** Immunofluorescence analysis of proplatelet formation by mature control (CNT) and GPIbα^{N103D} mutant MKs. The histogram presenting the frequency (%) of proplatelet forming MKs plated on the fibrinogen-coated surface in the presence or absence of ROCK1/2 inhibitor Y27632, for 24 hours. Data are expressed as mean±SEM, CNT: n=5, GPIbα^{N103D}: n=3, *P<0.05, ***P<0.001, One Way Analysis of Variance (ANOVA) with Tukey's multiple comparison method was used. Representative pictures of immunofluorescence staining are shown in SF 7B. **G-H.** 1.5x10^5 MKs were seeded in the silk scaffolds for 48 hours with or without the ROCK1/2 inhibitor Y27632, perfused with culture media for 6 hours, and released platelets were collected into gas-permeable bags **G.** The histogram represents the number of *ex vivo*-released platelets. Samples were mixed with counting beads to quantify the number of platelets identified as CD41$^+$CD42a$^+$ events. Data are expressed as mean±SEM, n=3, *P<0.05, **P<0.01, paired t-test. **H.** Platelet diameters (µm) of *ex vivo*-released platelets with or without ROCK1/2 inhibitor Y27632 were measured by Arivis Vision 4D (Zeiss). Data are expressed as mean±min to max, CNT: n=127, CNT+Y27632: n=133, GPIbα^{N103D}: n=136, GPIbα^{N103D} +Y27632: n=127, ****P<0.0001, One Way Analysis of Variance (ANOVA) with Tukey's multiple comparison method was used. Representative pictures of *ex vivo*-released platelets with or without ROCK1/2 inhibitor Y27632 are shown in SF 7C.

Figure 4. Mechanism of RhoA pathway activation.

A. Phosphoproteome analysis of control (CNT) and GPIbα^{N103D} mutant MKs. Mature MKs were seeded on fibrinogen-coated surface for 30 min, lysed and were analyzed using membrane-based human phospho-kinase antibody array. One of two experiments is shown. **B.** Western blot analysis of P-SRC Y419 and P-STAT3 Y705 in control (CNT) and GPIbα^{N103D} mutant MKs after 30 min incubation on fibrinogen-coated surface. Immunoblots were probed with mAbs directed against P-STAT3 Y705, P-SRC Y419, STAT3, SRC and Actin as loading control. Representative picture of immunoblot is shown on the left. Quantification of P-STAT3 Y705/total STAT3 is shown in the middle panel and that of P-SRC Y419/total SRC on the right panel. The ratios for mutant GPIbα^{N103D} MKs were normalized to control MKs. Data are expressed as mean±min to max, P-STAT3: n=7, P-SRC: n=8, *P<0.05, unpaired t-test. **C-E.** Effect of dasatinib on MK spreading. Control (CNT) and GPIbα^{N103D} mutant MKs were incubated in presence of dasatinib (10µM) for 15 min and plated on fibrinogen-coated

surface for 30 min. **C.** Western blot on MKs showing a decrease in P-SRC Y419 in CNT and GPIbα^{N103D} mutant MKs incubated with dasatinib. **D.** Representative pictures of stress fiber forming MKs stained with F-Actin (green) and DAPI (blue). Scale bar: 30µm, single z-stack frame at the glass adhesion site is shown. **E.** Frequency of stress fiber forming MKs. Data are expressed as mean±SEM, CNT: n=3, GPIbα^{N103D}: n=4, **P*<0.05, ***P*<0.01, One Way Analysis of Variance (ANOVA) with Tukey's multiple comparison method was used.

Figure 5. RhoA inhibition restores the platelet generation in heterozygous BSS.
Hematopoietic progenitors were isolated from peripheral blood of three healthy controls and one patient carrying heterozygous *GP1BA* p.L160P (P2) mutation, and cultured in presence of TPO and SCF for 10 days. **A-B.** Flow cytometry analysis of control (CNT1, CNT2) and patient 2 (P2) MKs. **A.** % of mature CD41^{+}CD42^{+} MKs. **B.** CD41 and CD42 expression level. **C-E.** MKs were seeded into the silk sponge with or without ROCK1/2 inhibitor Y27632. **C.** Representative picture of control (CNT2) and P2 proplatelet forming MKs. MKs and platelets are stained with anti-CD61 the antibody (green) and the silk sponge is in blue. Scale bar: 50µm, full 3D volume is shown. **D.** Silk scaffolds were perfused with culture media for 6 hours, and released platelets were collected into gas-permeable bags. Samples were mixed with counting beads to quantify the number of platelets, identified as CD41^{+}CD42a^{+} events. The number of recovered platelets is shown. A 1.48-fold increase in platelet number was detected for controls after incubation with ROCK1/2 inhibitor (n=3, data are presented as mean±SD) and 2.12-fold increase for P2 after incubation with ROCK1/2 inhibitor. **E.** Platelet diameters (µm) of *ex vivo*-released platelets with or without ROCK1/2 inhibitor Y27632 were measured by Arivis Vision 4D (Zeiss). Data are expressed as mean±min to max, n=50, *****P*<0.0001, One Way Analysis of Variance (ANOVA) with Tukey's multiple comparison method was used.

Figure 6. RhoA inhibition restores the platelet generation in heterozygous BSS.
Hematopoietic progenitors were isolated from peripheral blood of three healthy controls and one patient carrying heterozygous *GP1BA* p.N150S (P3) mutation respectively, and cultured in presence of TPO and SCF for 10 days. **A-C.** Flow cytometry analysis of control (CNT3) and patient 3 (P3) MKs. **A.** % of mature CD41^{+}CD42^{+} MKs. **B.** CD41 and CD42 expression level. **C.** Ploidy level. CD41^{+}CD42^{+} cells were incubated with Hoechst for 2 hours to label nucleus. N represents a mean ploidy level. **D.** MKs were seeded into the silk scaffold with or without ROCK1/2 inhibitor Y27632. *S*ilk scaffolds were perfused with culture media for 6 hours, and released platelets were collected into gas-permeable bags. Samples were mixed with counting beads to quantify the number of platelets, identified as CD41^{+}CD42a^{+} events. The number of recovered platelets is shown. A 4.67-fold increase was detected for P3 after incubation with ROCK1/2 inhibitor. **E.** Platelet diameters (µm) of *ex vivo*-released platelets with or without ROCK1/2 inhibitor Y27632 were measured by Arivis Vision 4D (Zeiss). Data are expressed as mean±min to max, CNT:n=57, CNT+Y27632:n=102, P3:n=57, P3+Y27632:n=57 *****P*<0.0001, One Way Analysis of Variance (ANOVA) with Tukey's multiple comparison method was used.

Figure 1

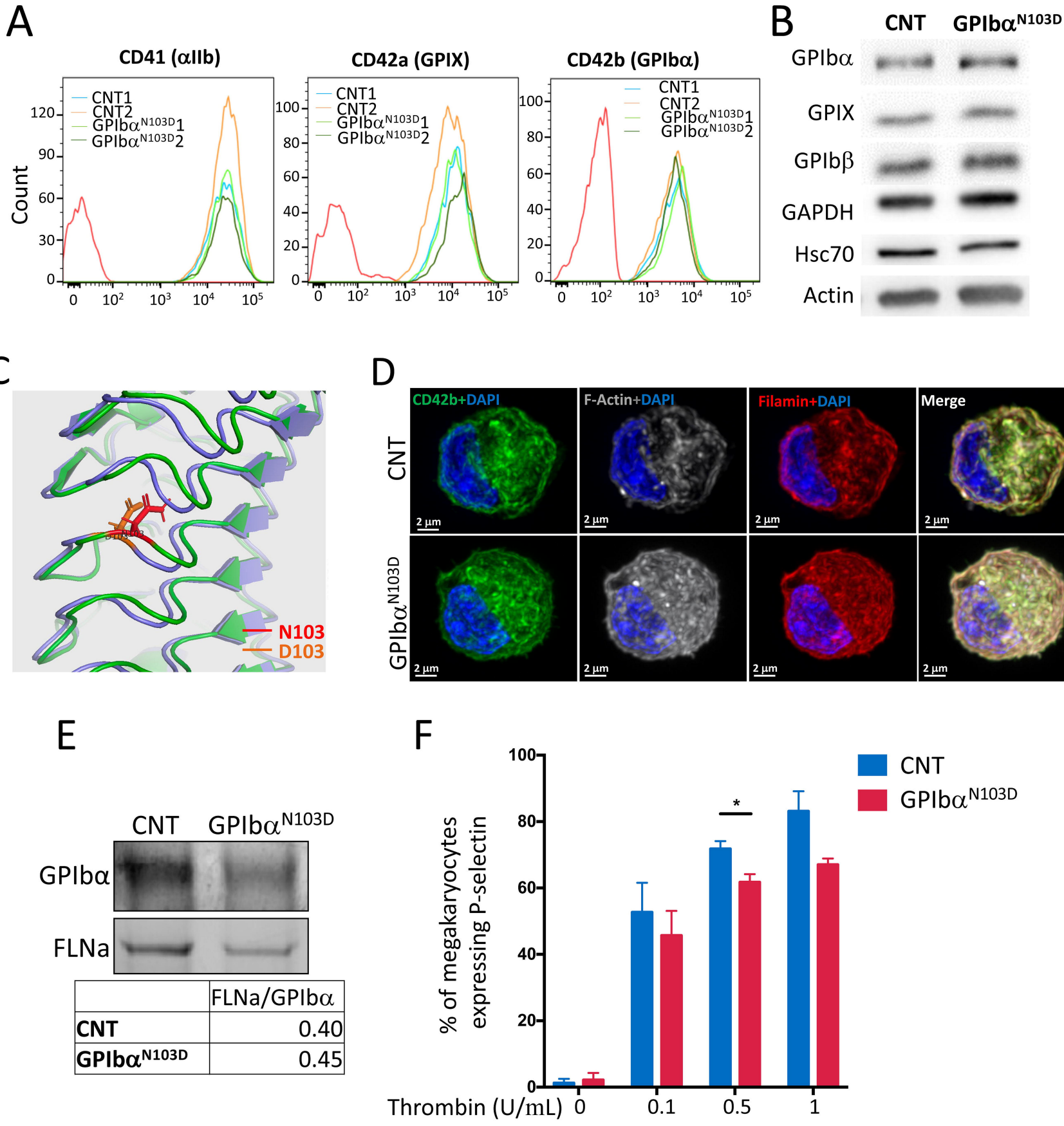
A
CD41 (αIIb)
CD42a (GPIX)
CD42b (GPIbα)
CNT1
CNT2
GPIbα^N103D1
GPIbα^N103D2
Count
B
CNT
GPIbα^N103D
GPIbα
GPIX
GPIbβ
GAPDH
Hsc70
Actin
C
N103
D103
D
CD42b+DAPI
F-Actin+DAPI
Filamin+DAPI
Merge
CNT
GPIbα^N103D
2 μm
E
CNT
GPIbα^N103D
GPIbα
FLNa
FLNa/GPIbα
CNT 0.40
GPIbα^N103D 0.45
F
% of megakaryocytes expressing P-selectin
CNT
GPIbα^N103D
*
Thrombin (U/mL) 0 0.1 0.5 1

Figure 2

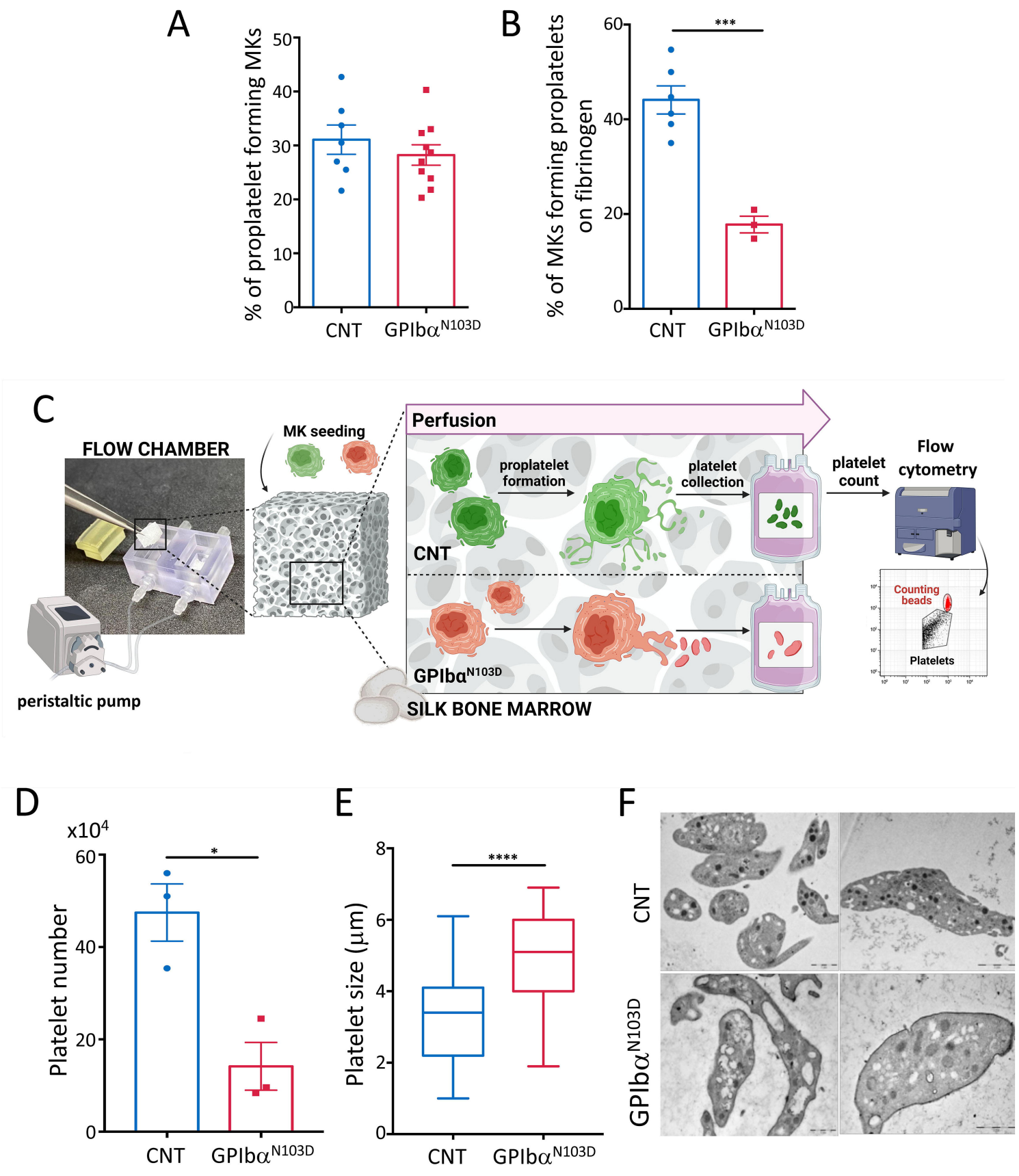
A
% of proplatelet forming MKs
50
40
30
20
10
0
CNT
GPIbα^N103D
B
% of MKs forming proplatelets on fibrinogen
***
60
40
20
0
CNT
GPIbα^N103D
C
FLOW CHAMBER
MK seeding
peristaltic pump
Perfusion
proplatelet formation
platelet collection
CNT
GPIbα^N103D
SILK BONE MARROW
platelet count
Flow cytometry
Counting beads
Platelets
D
x10^4
*
Platelet number
60
40
20
0
CNT
GPIbα^N103D
E
****
Platelet size (µm)
8
6
4
2
0
CNT
GPIbα^N103D
F
CNT
GPIbα^N103D

Figure 3

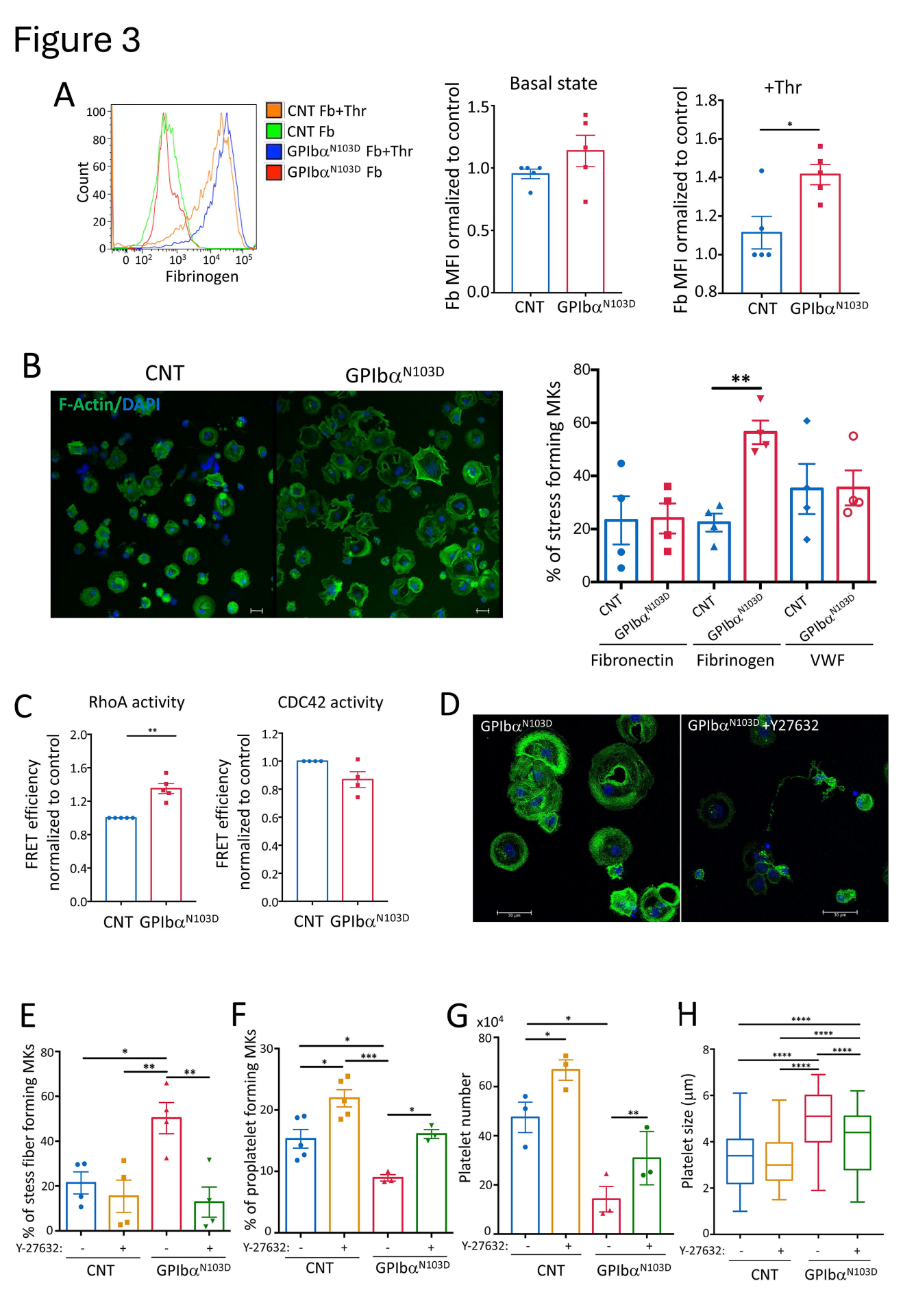
A
Count
Fibrinogen
CNT Fb+Thr
CNT Fb
GPIbα^N103D Fb+Thr
GPIbα^N103D Fb
Basal state
+Thr
Fb MFI ormalized to control
CNT
GPIbα^N103D
B
CNT
GPIbα^N103D
F-Actin/DAPI
% of stress forming MKs
Fibronectin
Fibrinogen
VWF
C
RhoA activity
CDC42 activity
FRET efficiency normalized to control
D
GPIbα^N103D
GPIbα^N103D +Y27632
E
% of stess fiber forming MKs
F
% of proplatelet forming MKs
G
Platelet number
x10^4
H
Platelet size (μm)
Y-27632:

Figure 4

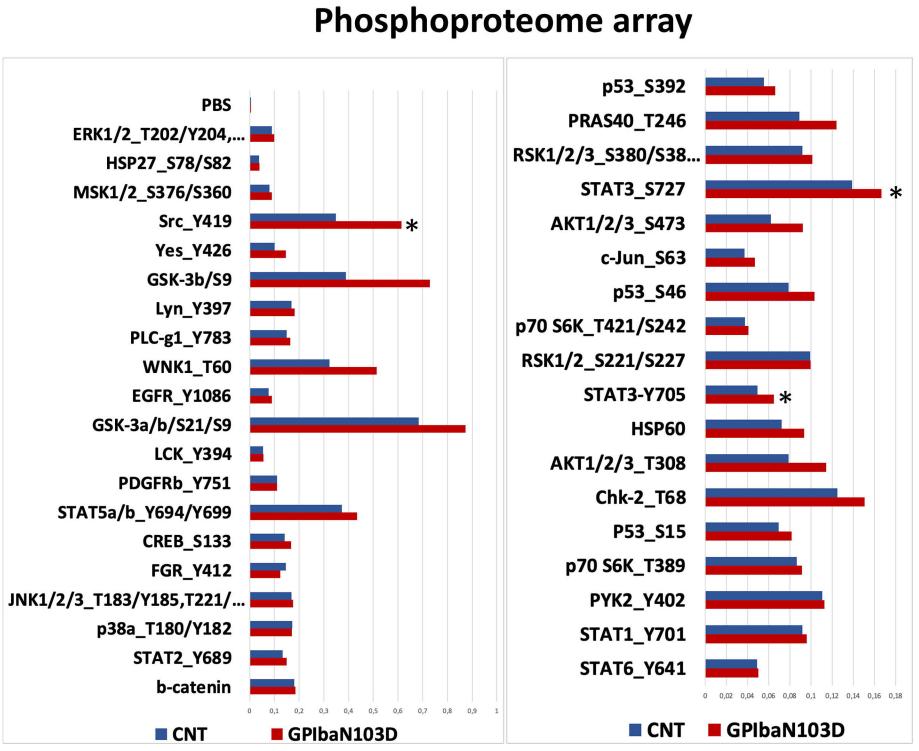
A
Phosphoproteome array
PBS
ERK1/2_T202/Y204,...
HSP27_S78/S82
MSK1/2_S376/S360
Src_Y419
Yes_Y426
GSK-3b/S9
Lyn_Y397
PLC-g1_Y783
WNK1_T60
EGFR_Y1086
GSK-3a/b/S21/S9
LCK_Y394
PDGFRb_Y751
STAT5a/b_Y694/Y699
CREB_S133
FGR_Y412
JNK1/2/3_T183/Y185,T221/...
p38a_T180/Y182
STAT2_Y689
b-catenin
CNT
GPIbaN103D
p53_S392
PRAS40_T246
RSK1/2/3_S380/S38...
STAT3_S727
AKT1/2/3_S473
c-Jun_S63
p53_S46
p70 S6K_T421/S242
RSK1/2_S221/S227
STAT3-Y705
HSP60
AKT1/2/3_T308
Chk-2_T68
P53_S15
p70 S6K_T389
PYK2_Y402
STAT1_Y701
STAT6_Y641
CNT
GPIbaN103D

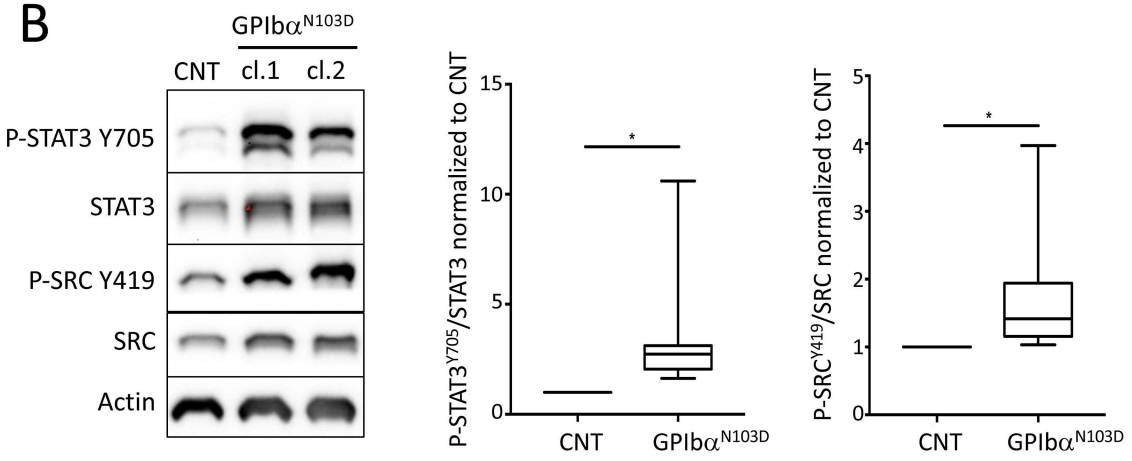
B
GPIbα^N103D
CNT
cl.1
cl.2
P-STAT3 Y705
STAT3
P-SRC Y419
SRC
Actin
P-STAT3^Y705/STAT3 normalized to CNT
CNT
GPIbα^N103D
P-SRC^Y419/SRC normalized to CNT
CNT
GPIbα^N103D

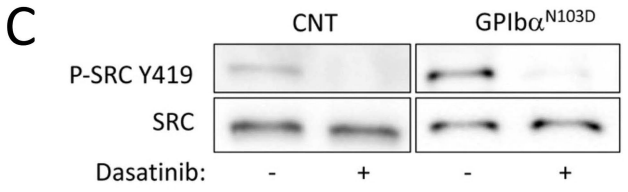
C
CNT
GPIbα^N103D
P-SRC Y419
SRC
Dasatinib:
-
+
-
+

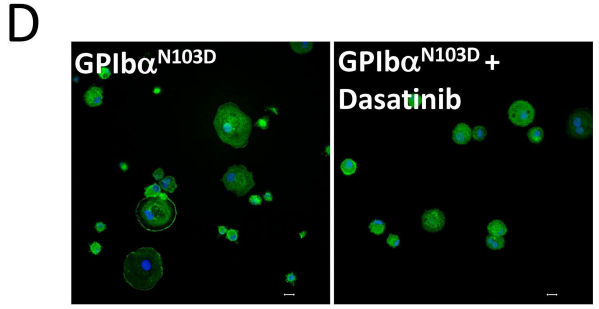
D
GPIbα^N103D
GPIbα^N103D + Dasatinib

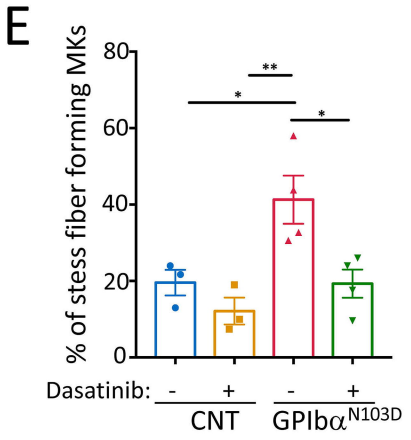
E
% of stess fiber forming MKs
Dasatinib:
-
+
-
+
CNT
GPIbα^N103D

Figure 5

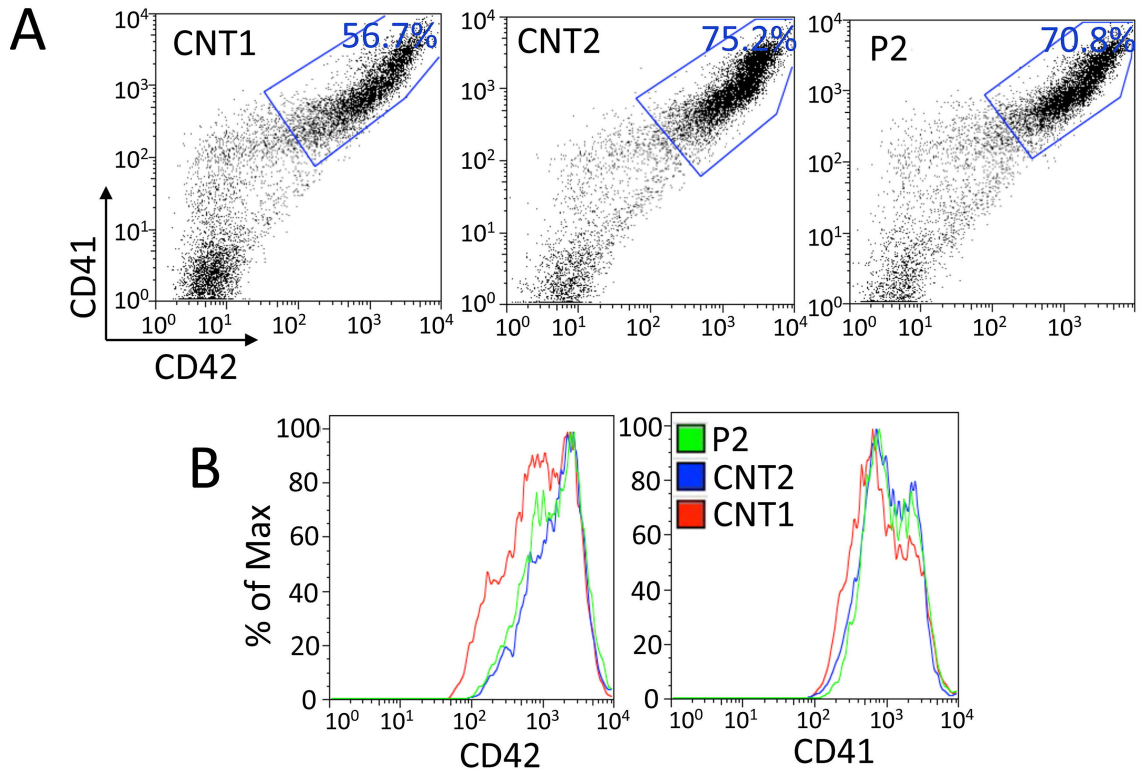
A
CNT1
56.7%
CNT2
75.2%
P2
70.8%
CD41
CD42
B
% of Max
P2
CNT2
CNT1
CD42
CD41

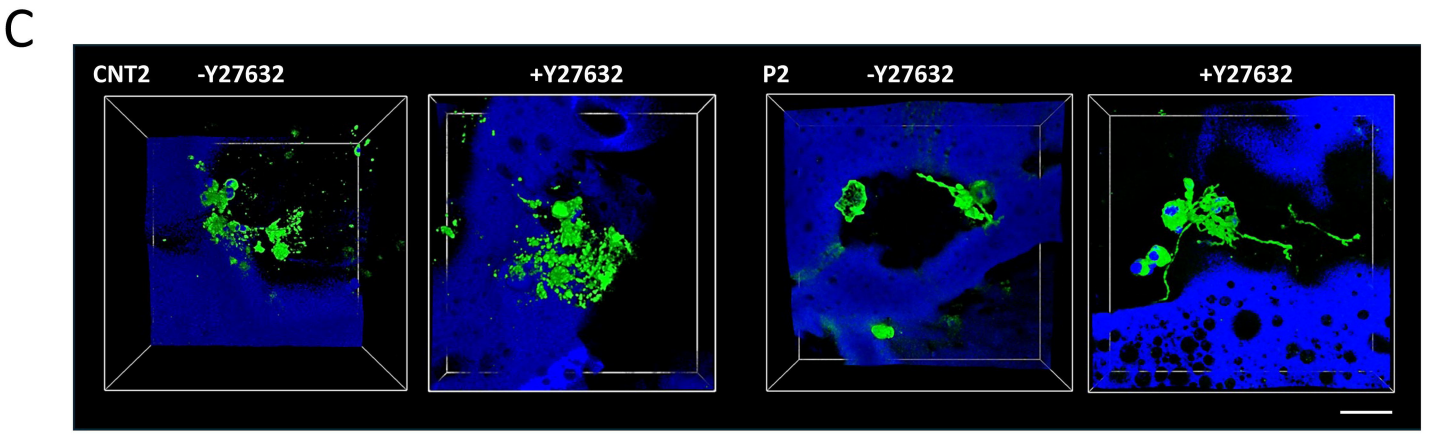
C
CNT2
-Y27632
+Y27632
P2
-Y27632
+Y27632

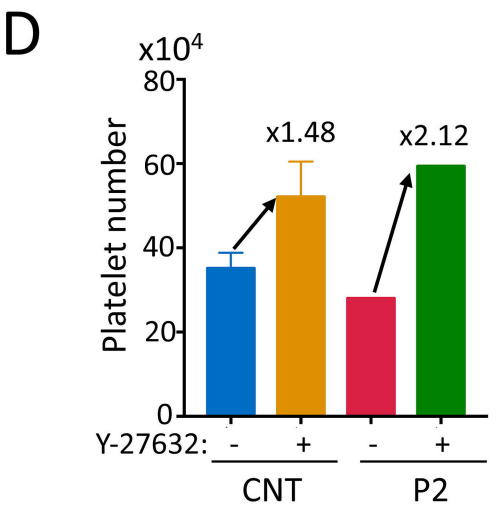
D
x10^4
Platelet number
x1.48
x2.12
Y-27632:
CNT
P2

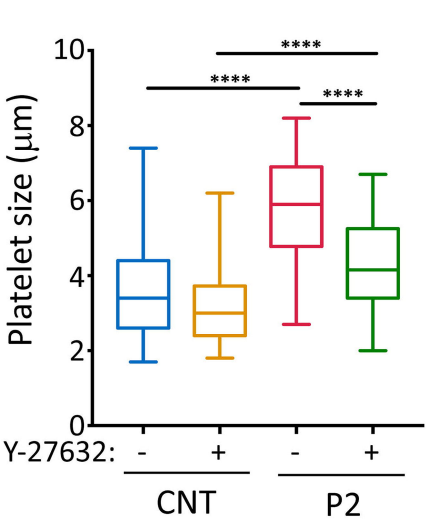
E
Platelet size (µm)
****
****
****
Y-27632:
CNT
P2

Figure 6

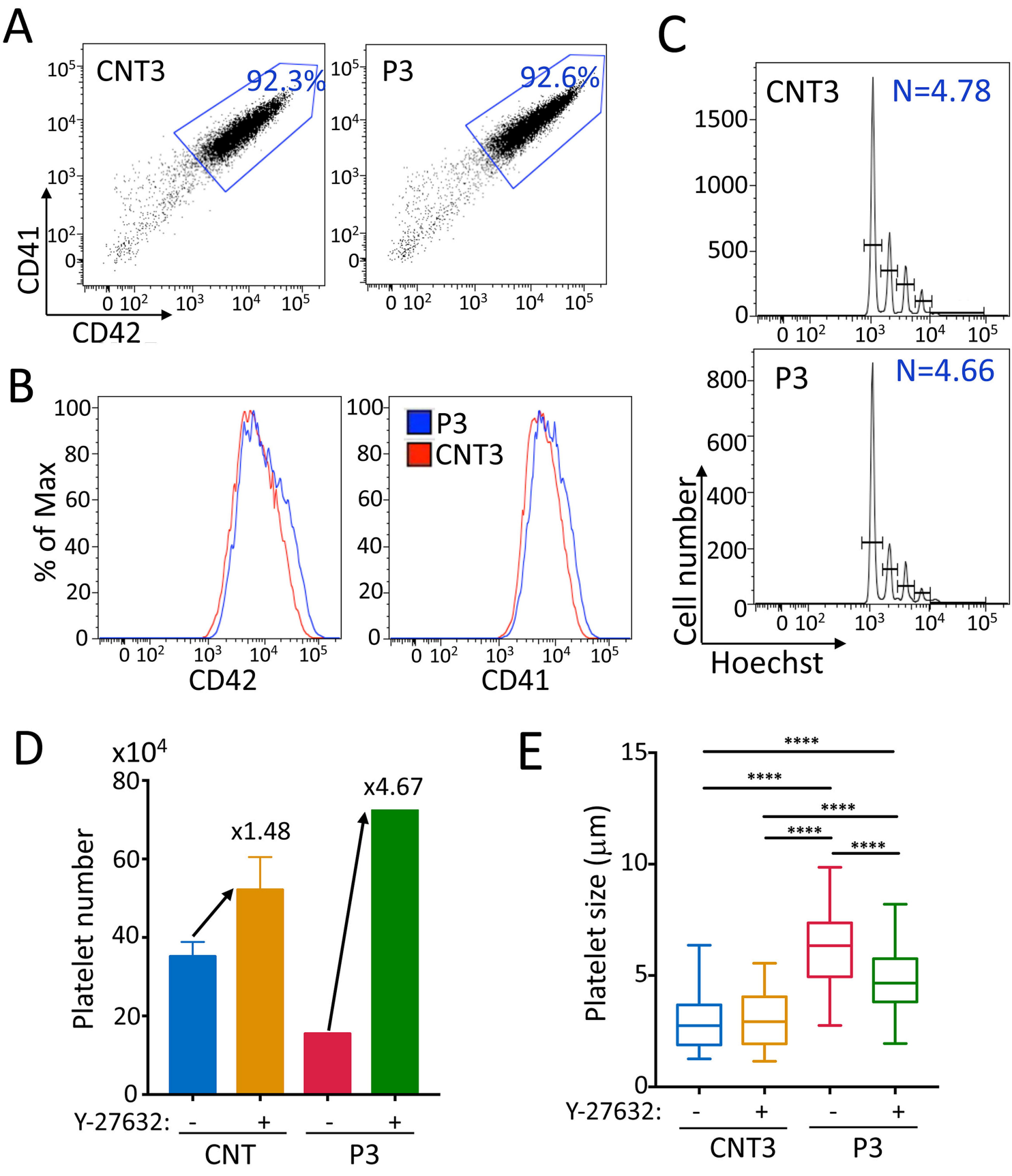
A
CNT3
92.3%
P3
92.6%
CD41
CD42
B
% of Max
P3
CNT3
CD42
CD41
C
CNT3
N=4.78
P3
N=4.66
Cell number
Hoechst
D
x10^4
Platelet number
x1.48
x4.67
Y-27632:
CNT
P3
E
Platelet size (µm)
****
Y-27632:
CNT3
P3

SUPPLEMENTAL FILE

MATERIAL AND METHODS

Bernard-Soulier syndrome patients

Five unrelated individuals (P1-P5) were identified with macrothrombocytopenia during routine blood tests. Upon further investigation, they were diagnosed with monoallelic (P1, P2, P3) or biallelic BSS (P4, P5). The diagnosis was confirmed through the identification of decreased ristocetin-induced aggregation and significant reductions in the platelet GPIb-V-IX complex (Cytoquant assay from Biocytex, Marseille, France) and by NGS. Platelet aggregation in response to 5-10 µM ADP, 5 µM epinephrine, 1-2.5 µg/mL collagen, 0.8-1 mM arachidonic acid, 10-25 µM TRAP and 1.5mg/L of ristocetin was performed as previously described[1] and expressed as maximal light transmission percentage (**ST1**). $CD34^+$ cells were isolated by a positive selection using an immunomagnetic cell sorting system (AutoMacs; Miltenyi Biotec, Bergisch Gladbach, Germany) and were cultured in serum-free medium containing TPO (10 ng/mL), SCF (25 ng/mL). For ploidy analysis, Hoechst 33342 (10 µg/mL; Sigma) was added in the medium at day 10 of culture for 2 h at 37C. Cells were then stained with directly coupled MoAbs: anti-CD41 APC and anti-CD42 PE (BD Biosciences) for 30 min at 4C. Ploidy was measured in the $CD41^+/CD42^+$ cell population by Fortessa (Becton Dickinson). The mean ploidy of human megakaryocytes (MKs) was calculated by the following formula: (2N x the number of cells at 2N ploidy level + 4N x the number of cells at 4N ploidy level+…+64N x the number of cells at 64N ploidy level /the total number of cells). For the analysis of proplatelet formation or platelet production, the $CD41^+CD42^+$ cells were sorted (FacsDIVA, Becton Dickinson, le Pont de Claix, France) on day 10 of culture and processed as described below.

iPSCs generation and expansion

$CD34^+$ cells were obtained from peripheral blood of P1 patient through positive selection using an immunomagnetic bead cell-sorting system (AutoMacs; Miltenyi Biotec). Subsequently, these cells were cultured in a serum-free medium that included EPO (1 U/mL), FLT3- L (10 ng/mL), G-CSF (20 ng/mL), IL-3 (10 ng/mL), IL-6 (10 ng/mL), SCF (25 ng/mL), TPO (10 ng/mL), and GM-CSF (10 ng/mL) for 6 days. Following this expansion phase, the cells underwent transduction using the CytoTune iPS 2.0 Sendai Reprogramming Kit (Thermo Fisher), and the reprogramming process was carried out according to the manufacturer's instructions. Colonies exhibiting an embryonic stem (ES)-like morphology were manually isolated, expanded for a reduced number of passages, and then cryopreserved. The induced

pluripotent stem cells (iPSCs) were cultured in StemMACS iPS-Brew medium (Miltenyi Biotech) on plates coated with N-truncated Human recombinant Vitronectin (Gibco). Regular cell passages were carried out using a 500 mM EDTA solution in 1X PBS. Routine Mycoplasma screening, following the manufacturer's instructions (Sigma), was performed. To minimize the risk of karyotypic and genomic anomalies, cells were maintained for a limited number of passages in culture.

qRT-PCR analysis of pluripotency markers

The validation of self-renewal stem cell markers (*SOX2*, *OCT4* and *NANOG*) was conducted through qRT-PCR analysis. The DDCt method was employed on the Rotor-Gene Q system (Qiagen) using the Maxima SYBR Green qPCR Master Mix (ThermoFisher Scientific). GAPDH was chosen as the housekeeping gene, and the data were normalized to its expression. Statistical analysis was carried out using the REST (Relative Expression Software Tool) software. The expression of self-renewal stem cell markers in GPIbα^{N103D} clones was compared to that in hESCs RC17 (Rosalin Cells, Edinburgh, UK) and hiPSCs CTR2#6.

Karyotype Analysis

On the 4th day post-split, induced pluripotent stem cells (iPS-cells) underwent a 3-hour treatment with 0.1 μg/mL Colcemid. A total of 32 to 38 metaphases were examined, and among them, 13-15 metaphases were karyotyped using QFQ-banding. The q-Bands were visualized through Fluorescence using Quinacrine and observed with a Fluorescence Microscope Olympus CHB (BX63) equipped with a quinacrine mustard filter and CCD camera. The analysis was performed using Bright-Field Microscope "GenASIs" Software, version 8.1.0.47741, developed by Applied Spectral Imaging.

Short Tandem Repeat (STR) Testing Report

Polymerase chain reaction (PCR) was employed to amplify nine autosomal short tandem repeat (STR) molecular markers (D21S11, D7S820, CSF1PO, TH01, D13S317, D16S539, vWA, TPOX, D5S818) along with the gender-determining marker Amelogenin, utilizing the Promega GenePrint 10 Kit as per the manufacturer's recommended protocol. Positive and negative amplification controls were included following the kit's guidelines. The resulting amplified products were subjected to analysis on an ABI Prism® 3730xl Genetic Analyzer, utilizing an

Internal Lane Standard 600 (Promega). Data generated were then analyzed using GeneMapper® Software version 4.0 (Applied Biosystems) in accordance with the manufacturer's instructions.

iPSCs hematopoietic differentiation

Clusters of pluripotent cells were seeded on Geltrex (Gibco)-coated plates in the presence of IPS-Brew medium at day -1. The initial cell concentration was adjusted for each cell line to achieve a 10-20% confluency range. On Day 0, cells were transferred to a xeno-free medium based on StemPro-34 SFM (Gibco), supplemented with 1% v/v Penicillin/Streptomycin (Gibco), 1% v/v L-Glutamine (Gibco), 0.04 mg/mL 1-Thioglycerol (Sigma), and 50 µg/mL ascorbic acid (Sigma). This medium was maintained throughout the experiment and supplemented with various cytokines and growth factors according to the following schedule:

- Days 0 – 2: BMP4 (10 ng/mL), VEGF (50 ng/mL), and CHIR99021 (2 µM).
- Days 2 – 4: BMP4 (10 ng/mL), VEGF (50 ng/mL), and bFGF (20 ng/mL).
- Days 4 – 6: VEGF (15 ng/mL) and bFGF (5 ng/mL).
- Day 6: VEGF (50 ng/mL), bFGF (50 ng/mL), SCF (25 ng/mL), and FLT3L (5 ng/mL).
- Days 7-10: VEGF (50 ng/mL), bFGF (50 ng/mL), SCF (25 ng/mL), FLT3L (5 ng/mL), TPO (25 ng/mL), and IL-6 (10 ng/mL).
- Days 10-20: SCF (25 ng/mL) and TPO (25 ng/mL).

Manufacturers of the components are detailed in Supplemental Table 2 (**ST2**).

Flow Cytometry

Single cell suspensions were subjected to staining using monoclonal antibodies directly coupled to their respective fluorochromes, as listed in **ST3**. The antibodies were applied to cells at a concentration of 1 µL per 10^6 cells in approximately 100 µL, and the incubation was carried out at 4°C for at least 30 minutes. Both before and after incubation, cells were washed with PBS 1X. Analysis was conducted using BD Canto II or BD LSRFortessa cytometers (BD Biosciences). For the isolation of MKs, Fluorescence Activated Cell Sorting (FACS) was routinely employed and executed on Influx, ARIA III, or ARIA Fusion cell sorters (BD Biosciences).

Proplatelet formation assay

Proplatelet formation was evaluated either on MKs cultured in a serum-free medium containing TPO (10 ng/mL) and SCF (25 ng/mL) or after 2-3 days adhesion on fibrinogen (20 µg/mL) by enumerating no less than 200 cells per well, utilizing an inverted microscope (Carl Zeiss) at a 200x magnification.

Immunoblot analysis

Cells: Cell lysis was carried out using 2x Laemmli buffer supplemented with a cocktail of protease inhibitors. Following lysing, proteins underwent separation by SDS-PAGE and were subsequently transferred onto nitrocellulose membranes. The membranes were blocked for 1 hour using a 5% w/v BSA solution in Tween-PBS 1X. Primary antibodies were then incubated overnight, followed by a 1-hour incubation with secondary antibodies coupled to horseradish peroxidase. Both types of antibodies were diluted in a solution of 5% w/v BSA in Tween-PBS 1X. Primary and secondary antibodies, including clone names, concentrations, and manufacturers, are listed in Supplemental table 3 (**ST3).**

Supernatant: To analyze soluble GPIbα in the culture medium, 150 000 ($CD41^+CD33^-$) MKs were sorted on day 13 of culture, seeded in 150 µl of serum-free medium containing TPO and SCF and four days later, the cells were centrifuged at 3000 rpm to remove all cells and cellular debris. 10 µl of supernatant was used for WB analysis. Recombinant soluble GPIbα $(rGPIb)^2$ was used as a control.

Band detection was performed by enhanced chemiluminescence system (ECL or SuperSignal West Pico Plus kit; Life Technologies) using Image Quant LAS 4000 (GE Healthcare)/iBright FL1500 (Thermo Fisher Scientific). The quantification was by ImageJ2 software.

Immunoprecipitation assay

iPSC were lysed with lysis buffer containing 1% Triton X-100, 150 mM NaCl, 50 mM Tris pH 7.4, 5 mM EGTA, 1 mM Na_3VO_4, 1x Halt Protease Inhibitor Cocktail. GPIbα was precipitated by incubation of the lysates with an anti-GPIbα antibody (clone SZ2, 2 µg)-coated protein G-magnetic beads 1h at RT. Supernatant was collected and the magnetic beads were washed 3 times with 1x lysis buffer before 2x Laemmli buffer was added. Samples were separated by SDS–PAGE.

Proteome Phospho-Kinase Array

The impact of a fibrinogen binding to αIIbβ3 on the phosphorylation of kinases in MKs was investigated using a membrane-based human phospho-kinase antibody array kit (ARY003B, R&D Systems, Minneapolis, MN, USA), designed to profile 46 specific phosphorylation sites. According to the manufacturer's instructions, mature MKs were plated on a fibrinogen-coated surface for 30 minutes at 37°C. Subsequently, the corresponding cell lysates were incubated with the pre-blocked membrane overnight at 4 °C. On the following day, the membrane underwent extensive rinsing and was then incubated with biotinylated detection antibodies (antibody cocktail) at room temperature for 2 hours. Following this, the membrane was exposed to a diluted streptavidin-horseradish peroxidase (HRP) solution at room temperature for 30 minutes, and visualization was achieved using a chemi-reagent mix. Detection and quantification of pixel density for the obtained spots were performed using Image Quant LAS 4000 (GE Healthcare) and ImageJ software Version 1.51n, respectively. The results were expressed as the relative phosphorylation level of the corresponding kinase.

Von Willebrand Factor binding assays

Purified MKs underwent incubation with human von Willebrand Factor (VWF) at concentrations ranging from 0 to 0.5 μg/mL in the presence of the VWF-modulator ristocetin (0.5 mg/mL) for 15 minutes at room temperature. Following this, cells were fixed with 1% paraformaldehyde for 5 minutes. Washed cells were then treated for 30 minutes with an anti–human VWF-specific monoclonal antibody (mAb) and subsequently with Alexa Fluor 488–anti-Rabbit Antibody. Flow cytometry was employed for analysis. To block VWF binding to human GPIbα, the anti–human GPIbα-specific monoclonal antibody SZ2 (0.5 or 1μg) was utilized. MKs were preincubated for 15 minutes with the anti–human GPIbα blocking antibody before incubation with human VWF, following the previously described treatment. The antibodies used are listed in Supplemental Table 2 (**ST3**).

aIIbβ3 activation assay

The activation of integrin αIIbβ3 was assessed through flow cytometry. MKs were suspended in Tyrode's buffer, incubated with either Alexa Fluor 647-labeled PAC1 antibody or Alexa 488-labeled Fibrinogen, in the presence or absence of thrombin (1U/mL) for 5 minutes at 37°C. Following this, cells were fixed with 1% paraformaldehyde and analyzed on a BD Canto II flow

cytometer (BD Biosciences, Franklin Lakes, NJ, USA). The antibodies used are listed in Supplemental Table 3 (**ST3**).

Immunofluorescence microscopy and fluorescence quantification

Mature MKs were plated on poly L-lysine-coated slides, for 1 hour at 37°C, or cultured in adhesion onto fibrinogen, as described above. Subsequently, they were fixed with 4% paraformaldehyde, permeabilized using 0.1% Triton X-100, and stained with anti-β-tubulin, anti-P-MLC2, anti-FLNa, anti-CD42b, or anti-VWF antibodies. This was followed by incubation with secondary Alexa Fluor-488 goat anti-mouse or anti-rabbit antibodies, Alexa Fluor 555–phalloidin or Alexa Fluor 488-phalloidin or Alexa Fluor 633-phalloidin and DAPI for visualization of specific cellular components. A detailed list including the concentration, clone name, and manufacturer for each antibody can be found in Supplemental Table 3 (**ST2**).

Coverslips were mounted in Mowiol for observation under a confocal microscope Leica SP8 (Danaher Corporation, objective 63XNA1.40) using LAS acquisition software (AF version 1.62; Leica). Image analysis was subsequently performed with the LASX software. To quantify the distribution of fluorescent signal between different experimental conditions and to measure the area of pro-platelet tips, confocal microscopy images were analyzed using Fiji software (ImageJ 2.1.0). The analysis workflow involved several steps: 1) Image Preprocessing: Confocal images were opened in Fiji (.lif format), the "Split Channels" function was used to separate the four fluorescence channels. For each channel, a Z-stack projection was created using the "SUM" method to generate a single image representing the total intensity across the Z-stack. 2) Region of Interest (ROI) Definition: *Membrane ROI:* Four rectangular ROI were defined for each image and placed at the edge of the cell, including the membrane and slightly encompassing the cytoplasm. *Nuclear-Excluding Cytoplasmic ROI:* A square ROI placed at the center of the cell, avoiding the nucleus region. *Tip ROI:* For pro-platelet tip area measurement, a separate ROI was created encompassing the tip of the pro-platelet. 3) Thresholding: An automatic Otsu thresholding method[3] was applied to each ROI to separate the fluorescent signal from the background. This method dynamically sets the threshold based on the image histogram, ensuring optimal signal segmentation. 4) Fluorescence Intensity Measurement: The mean fluorescence intensity was measured for each ROI and fluorescence channel. This provided quantitative data on the distribution of fluorescent signal within the membrane/cytoplasm and nuclear-excluding region. 5) Pro-Platelet Tip Area Measurement: The area of the pro-platelet tip ROI was measured in microns squared. 6) Data Analysis: The

data was collected from at least 11 cells per experimental condition (4 conditions in total, 2 different controls and 2 different GPIbα^{N103D} clones). The ratio between the mean intensity in the membrane ROI and the nuclear-excluding cytoplasmic ROI was calculated for each cell and condition. This ratio provided a measure of the relative distribution of fluorescent signal within the cell. For the analysis of proplatelet tips, the area of tips was analyzed and fluorescence measurements were calculated per 1μm^2 and compared between different conditions.

MK spreading and stress fiber formation

Slides were coated with human VWF (1 μg/mL) and ristocetin (0.5 mg/mL), fibrinogen (20 μg/mL), or fibronectin (25 μg/mL) in PBS buffer overnight at 4°C. They were subsequently blocked with BSA (5 mg/mL) for 1 hour at room temperature and washed with PBS before use. Mature MKs were then plated on surfaces coated with fibronectin, fibrinogen, or VWF for 30 minutes at 37°C. In experiments involving dasatinib, mature MKs were incubated for 15 minutes with dasatinib (10 μM) and then plated on a fibrinogen-coated surface for 30 minutes at 37°C. For experiments involving the ROCK1/2 inhibitor, MKs were plated with or without Y27632 (10 μM) on a fibrinogen-coated surface for 30 minutes at 37°C. In experiments with thrombin, thrombin (1U/mL) was added to the cell suspension and immediately after, MKs have adhered on fibrinogen. Adhered MKs were fixed with 4% paraformaldehyde, permeabilized using 0.1% Triton X-100, and stained with Alexa Fluor 488–phalloidin and DAPI. A detailed list containing the concentration, clone name, and manufacturer for each antibody can be found in Supplemental Table 2 (**ST2**). The adhesion and spreading of MKs were visualized using differential interference contrast (DIC) microscopy (DMIRB, 63× or 100× Objective; Leica), and images were captured using DVT tools (Pinnacle Systems). Image analysis was subsequently performed with the LASX software. Quantification of the number of adherent and spreading MKs was conducted by analyzing at least three random fields.

Preparation of silk fibroin scaffolds

Silk fibroin aqueous solution was obtained from *B. mori* silkworm cocoons according to previously published literature.[3] Briefly, fibroin was obtained by boiling cocoons in Na_2CO_3. The fibers were rinsed in ultrapure water and dried at room temperature (RT) for 48 h. The dried fibers were subsequently solubilized in Lithium Bromide solution for 4 h at 60 °C. The silk solution was then dialyzed against deionized water using a Slide-A-Lyzer cassette (Thermo

Fisher). Silk scaffolds have been produced by a salt-leaching method and functionalized with 50 µg/mL fibrinogen or 50 µg/mL fibronectin, as previously described.[4-7]

Silk bone marrow assembly and perfusion

The dynamic perfusion of the silk bone marrow scaffold was performed by using a peristaltic pump (ShenChen Flow Rates Peristaltic Pump - LabV1) connected to a bioreactor chamber manufactured using 3D SLA printing technology (Form 3B (Formlab)). The chamber was designed using CAD software (Fusion 360). The printing was performed using the Biomed Clear biocompatible resin cured in layers of 100 µm. The resulting chamber was washed with isopropyl alcohol (IPA) to remove the unpolymerized resin and then cured in a UV oven for 1 h. The resulting flow chamber consisted of two wells of 10 (L) × 5 (W) × 5 (H) mm having independent inlets and outlet channels. Each well was equipped with a silk fibroin scaffold. 1.5×10^5 MKs were seeded into each silk scaffold and kept at 37 °C and 5% CO_2. Scaffolds have been sterilized and rinsed in the culture medium before cell seeding.

Flow cytometry analysis of platelets

Flow cytometry settings for *ex vivo* generated platelets were established, as previously described.[5-7] Briefly, *ex vivo* collected platelets were analyzed using the same forward and side scatter pattern as human peripheral blood and identified as $CD41^+CD42a^+$ events. Isotype controls were used as a negative control to exclude non-specific background signals. The platelet number was calculated using a Tru-Count bead standard (Beckton Dickinson). Samples were acquired using a BD FACS Lyric (Becton Dickinson) or BD Canto II flow cytometer (Becton Dickinson). Off-line data analysis was performed using Kaluza software package (Beckman Coulter) or FlowJo v9.3.2 software (Becton Dickinson).

Imaging of the 3D silk bone marrow model

For immunofluorescence imaging within the silk bone marrow scaffold, samples were fixed in 4% PFA for 20 min and then blocked with 5% bovine serum albumin (BSA, Sigma) for 30 min at RT. Samples were stained with anti-CD61 (#IM0540) (1:100) (Beckman Coulter) diluted in 1% BSA, overnight at 4 °C. Then, samples were immersed in Alexa Fluor secondary antibody (1:200) diluted in 1% BSA for 2 hours at RT. Nuclei were stained with Hoechst. Silk fibroin fluorescence was brightened by Hoechst.[7] 3D reconstructions and image processing were performed using Leica LasX (Leica) and Arivis Vision 4D (Zeiss). Platelet diameters were

measured by Arivis Vision 4D (Zeiss). The analyses of samples have been performed blinded to genotype.

Transmission electron microscopy

MKs were fixed in 2% glutaraldehyde in 0.1M phosphate buffer for 1 hour at 4°C and postfixed with 2% osmium tetroxide in 0.1M phosphate buffer for 1 hour at room temperature. After dehydration through a graded ethanol series, samples were embedded in Epon™ 812, and polymerization was completed after 48 hours at 60 °C. Ultrathin sections were stained with standard uranyl acetate and lead citrate and observed with a FEI Tecnai 12 electron microscope. Digital images were captured using a SIS MegaviewIII CCD camera.

FRET analysis

The lentiviral RhoA or Cdc42 FRET sensors (pPBbsr2-Raichu-2707x, pRaichuEV-Cdc42-KRasCT pCSIIbsr-2280x) were generously provided by Dr. Matsuda. Viral particles were produced following the procedure as previously described.[8] MKs derived from induced pluripotent stem (iPS) cells were transduced, and cells expressing CFP and YPet were selected through FACS. Subsequently, the transduced MKs were plated on a fibrinogen-coated surface for 30 minutes at 37 °C. Slides were mounted with Fluoromount-G® (Southern Biotech).

Förster resonance energy transfer (FRET) was performed on a confocal microscope Leica SP8 with a 63X objective (1.4 NA) using the acceptor photo-bleaching method through the FRET-AB wizard of the Leica software. Briefly, the acceptor fluorophore (YPet) fluorescence was bleached at 100% laser intensity, with a minimal extent of bleaching set at 75%. This resulted in an increased fluorescence intensity of the donor fluorophore (CFP) in the bleached region, which was subsequently measured. FRET efficiency was obtained using the formula:

$$FRET_{eff.} = \frac{CFP_{post} - CFP_{pre}}{CFP_{post}}$$

Statistics

All data are shown as mean ± SEM, mean±SD or as mean ± min to max. The statistical analyses were performed using the PRISM software. Statistical significance was established using a Student's *t* test or a One Way Analysis of Variance (ANOVA) specified in legends. Differences were considered significant at $P < 0.05$.

Supplemental Table 1

Patient	Mutation	Sex/age	Platelet count	ISTH-BAT score	Platelet aggregation (%)					
		(years)	(x10^9/L)		ADP	EPI	COL	AA	TRAP	Ristocetin
P1	GPIbα^{N103D} (heterozygous)	F/62	118	2	80	70	80	70	80	75
P2	GPIbα^{L160P} (heterozygous)	F/40	88*	0	60	50	50	65	65	50
P3	GPIbα^{N150S} (heterozygous)	F/12	90*	7	42	ND	41	41	50	49
P4	GPIbβ^{G43W} (homozygous)	F/11	50-130*	1	55	ND	57	60	53	60
P5	GPIbα^{L139P} (homozygous)	M/28	16*	7	59	ND	64	ND	55	<10

Supplemental table 1: Patient characterization

Patient features. ISTH-BAT: International Society on Thrombosis and Hemostasis-bleeding assessment tool; ADP: adenosine diphosphate; ATP: adenosine triphosphate; EPI: epinephrin; COL: collagen; AA: arachidonic acid; TRAP: thrombin receptor activating peptide.

* PRP< 150 G/L, the results could be innacurate, ND: not done

Platelet aggregation in response to ADP, EPI, COL, AA, TRAP and ristocetin is expressed as maximal light transmission percentage.

Concentration of ADP, COL 1, AA, TRAP, Ristocetin:

P1, P2: ADP 5mM, EPI 5mM, COL 1mg/mL, AA 1mM, TRAP 20mM, Ristocetin 1.5mg/L

P3: ADP 10 mM, COL 2.5mg/mL, AA 0.8mM, TRAP 25mM, Ristocetin 1.5mg/L

P4: ADP 10 mM, COL 1.2mg/mL, AA 1mM, TRAP 10 mM, Ristocetin 1.5mg/L

P5: ADP10 mM, COL 2.5mg/mL, TRAP 10 mM, Ristocetin 1.5 mg/L

Supplemental Table 2

Antibody or other reagent	Source	Identifier	Working Dilution
CD41a - APC	BD Biosciences	#559777 / HIP8	1:100 (flow cytometry)
CD42a - PE	BD Biosciences	#558819 / ALMA.16	1:100 (flow cytometry)
Oct3/4 - PerCP-Cy™5.5	BD Biosciences	#560794 / 40/Oct-3	1:100 (flow cytometry)
Sox2 - Alexa Fluor® 647	BD Biosciences	#560302 / 245610	1:100 (flow cytometry)
Nanog - PE	BD Biosciences	#560483 / N31-355	1:100 (flow cytometry)
IgM - APC	BD Biosciences	#555585 / G155 - 228	1:100 (flow cytometry)
IgG1 - PE	BD Biosciences	#555749 / MOPC-21	1:100 (flow cytometry)
IgG1 - PerCP-Cy™5.5	BD Biosciences	#552834 / MOPC-21	1:100 (flow cytometry)
IgG2a - Alexa Fluor® 647	BD Biosciences	#565365 / MOPC-21	1:100 (flow cytometry)
b-Tubulin	Sigma	#T8328 / AA2	1:200 (IF)
Phalloidin-FITC	Sigma	#P5282	1:400 (IF)
Phalloidin-Atto633	Sigma	#68825	1:400 (IF)
Actin	Sigma	#A5441 / AC-15	1:1000 (WB)
GAPDH	Santa Cruz Biotechnology	sc-32233	1:1000 (WB)
HSC70 (mAb, Clone: 6E1)	Active Motif	#61207	1:1000 (WB)
IgG anti-rabbit H+L Alexa Fluor 633	Thermo Fisher Scientific	#A-21071	1:400 (IF)
IgG anti-mouse H+L Alexa Fluor 546	Thermo Fisher Scientific	#A-11003	1:400 (IF)
IgG anti-rabbit HRP-linked	Cell Signaling Technology	#7074	1:2000 (WB)
IgG anti-mouse HRP-linked	Cell Signaling Technology	#7076	1:2000 (WB)
Src	Abcam	Ab109381	1 :10000 (WB)
Src (Y419)	Abcam	Ab185617	1 :5000 (WB)
Stat3	Cell Signaling Technology	#9132	1 :1000 (WB)
Stat3 (Tyr705) D3A7	Cell Signaling Technology	#9145	1:2000 (WB)
GPIBa (CD42b (MM2/174))	Santa Cruz Biotechnology	Sc80728	1 :500 (WB), 1 :200 (IF)
GPIBa (CD42b SZ2)	Sant Cruz Biotechnology	Sc-59052	1 :500-1:1000 (WB); 0.5 or 1 µg (VWF binding tests), 2 µg (IP)
GPV (CD42d G-11)	Sant Cruz Biotechnology	Sc-271662	1 :500 (WB)
GPIX (CD42a A-9)	Sant Cruz Biotechnology	Sc-166420	1 :500 (WB)
CD61	Beckman Coulter	#IM0540	1 :100 (IF)
PAC-1-FITC	Biolegend	A86877	1 :50 (Flow cytometry)
FLNA (C-TERM)	Abcam	#ab51217	1:200 (IF) – 1:1000 (WB)
VWF	Dako	A0082	1 :1000 (flow cytometry)
Fibrinogen Alexa Fluor 488	Invitrogen™	F13191	1 :200 (flow cytometry)
MLC-2 (Ser19)	Cell Signaling	#3671	1 :100 (IF), 1 :1000 (WB)
MLC-2	Cell Signaling	#3672	1 :1000 (WB)

Supplemental table 2: List of antibodies used, including source, identifier and working dilution

Supplemental Table 3

Reagent	Source	Identifier
hBMP4	Peprotech	#AF-120-05ET
hVEGF	Peprotech	#100-20
hFGF-basic	Peprotech	#100-18B
hIL-6	Peprotech	#200-06
hTPO	Kirin Brewery, Tokyo, Japan	/
hFLT3-L	Celldex Therapeutics, Inc., Needham, USA	/
hSCF	Biovitrum AB, Stockolm, Sweden	/
hEPO	Peprotech	#100-64
hG-CSF	Peprotech	#300-23
hGM-CSF	Peprotech	#300-03
hIL-3	Peprotech	#200-03
CHiR 99021 trihydrochloride	TOCRIS	#4953
Y-27632 dihydrochloride	TOCRIS	#1254
VTN-N	Gibco/Thermo Fisher Scientific	#A14700
Geltrex	Gibco/Thermo Fisher Scientific	#A1413202
StemMACS™ iPS-Brew XF, human	Miltenyi Biotec	130-104-368
StemPro®-34 SFM	Gibco/Thermo Fisher Scientific	#10639011
CytoTune™-iPS 2.0 Sendai Reprogramming Kit	Invitrogen/Thermo Fisher Scientific	#A16517
1-thioglycerol	Sigma	#M6145
Fibrinogen	Sigma	#F8630
Fitronectin	Gibco™/ Thermo Fisher Scientific	33016015
Dasatinib	Sigma	CDS023389
Hoechst 33342	Sigma	14533
Nocodazole	Sigma	M1404
Ristocetin	Clinisciences	C4176
von Willebrand Factor (WILFACTIN)	LFB	/

Supplemental table 3: List of reagents used, including source and identifier

Supplemental Figure 1

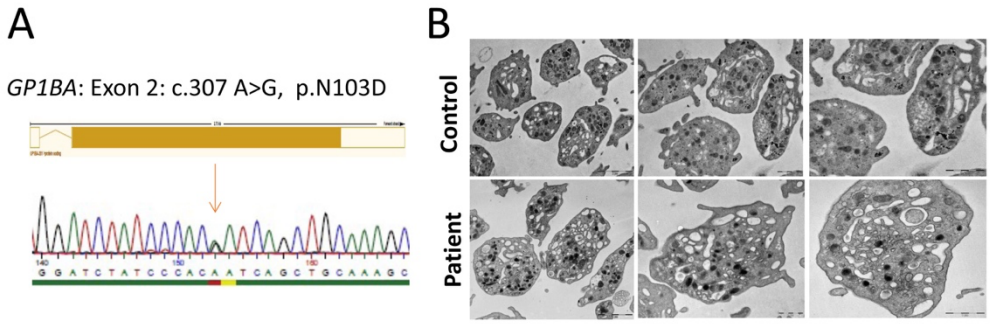

Supplemental Figure 1. Characterization of the patient's blood platelets and *GP1BA* gene mutation. A. Sanger sequencing confirming the heterozygous c.307A>G substitution in *GP1BA* leading to a p.Asn103Asp (p.N103D) change within LRR4 of GPIbα. **B.** Transmission electron microscopy (TEM) of the patient's and control platelets. For the patient, platelets are of increased size.

Supplemental Figure 2

A

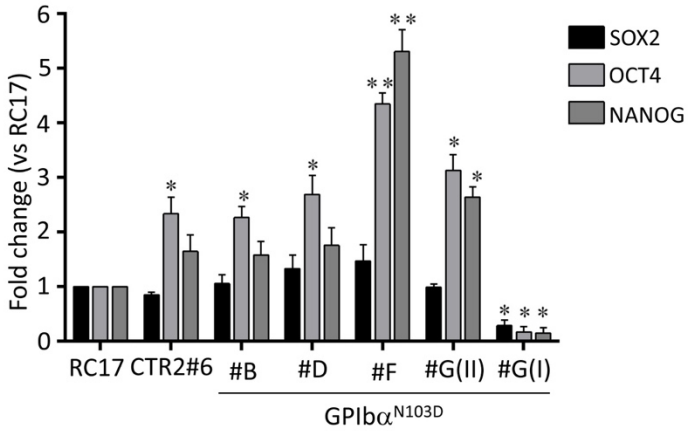

B

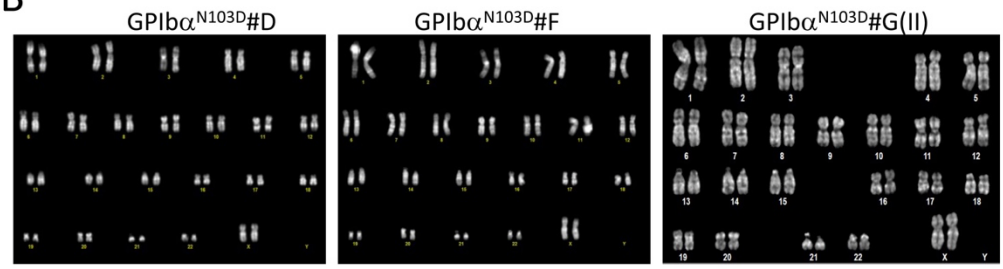

C

Locus Repeat	#STR Genotype		
	GPIBα^{N103D}#D	GPIBα^{N103D}#F	GPIBα^{N103D}#G(II)
TH01	7, 8	7, 8	7, 8
D21S11	31.2, 32.2	31.2, 32.2	31.2, 32.2
D5S818	12, 12	12, 12	12, 12
D13S317	12, 13	12, 13	12, 13
D7S820	12, 12	12, 12	12, 12
D16S539	11, 11	11, 11	11, 11
CSF1PO	11, 12	11, 12	11, 12
AMEL	X, X	X, X	X, X
vWA	17, 17	17, 17	17, 17
TPOX	8, 11	8, 11	8, 11

Supplemental Figure 2. Characterization of GPIbα iPSC clones B, D, F, GI, GII. A. qRT-PCR analysis of *SOX2*, *OCT4* and *NANOG* transcripts relative to *GAPDH* housekeeping gene and normalized to control line hESCs RC17 cell line. Clone GI expressed lower levels of pluripotency markers than control cell line and was not used for further experiments. **B.** Karyotype analysis showing normal 46, XX karyotype for D, F, GII GPIba iPSC clones. Clone B revealed karyotypic anomalies (not shown) and was not used for further experiments. 32 to 38 total metaphases were analyzed and 13-15 total metaphases were karyotyped by Q-binding method with resolution of 350 bands. **C.** Short Tandem Repeat (STR) Testing Report.

Supplemental Figure 3

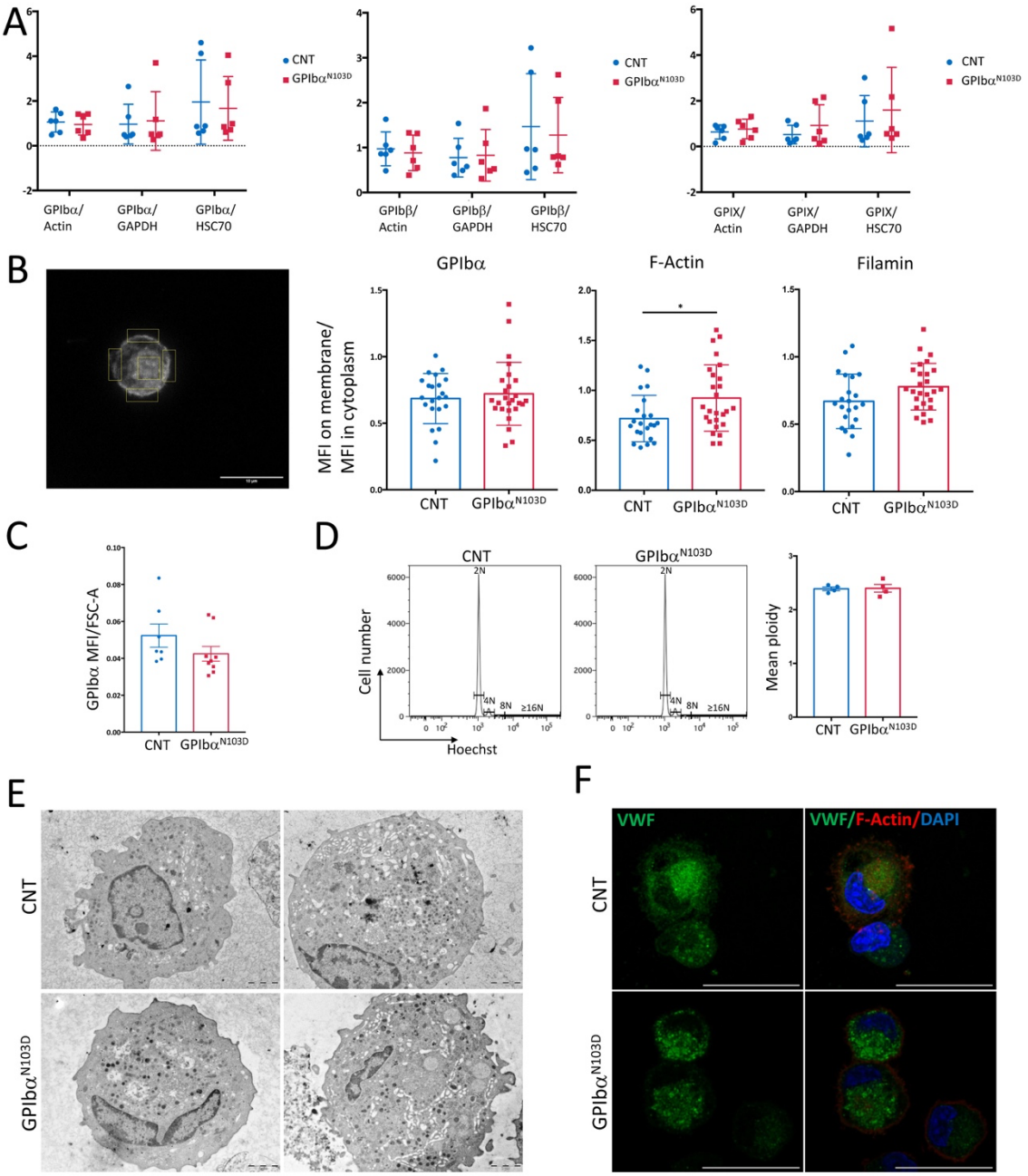

Supplemental Figure 3. GPIbα^{N103D} mutant does not affect the expression of GPIb/GPIX complex and megakaryocyte differentiation from iPSC. A. Western blot analysis and quantification of GPIbα, GPIbβ and GPIX relative to three houskeeping proteins, Actin, GAPDH and HSC70. The histograms show quantification of the WBs representing averages of 3 independent experiments performed each on two independent CNT and GPIbα^{N103D} clones as mean±SD, unpaired t-test. **B.** Fluorescence analysis of CD42b (GPIbα); F-Actin and Filamin distribution in MKs. On the left: a representative picture of MK with rectangles and square depicting the areas of fluorescence measurement, z-stack middle frame is shown. On the right: the histograms presenting the quantification of GPIbα, F-Actin and Filamin. The ratio between Mean Fluorescence Intensity (MFI) measured on membrane and MFI measured in the center of cell is shown as mean±SD, *P<0.05, unpaired t-test. At least 11 MKs were analyzed for each

of two controls (CNT) and two GPIbα^{N103D} clones. **C.** Quantification of GPIbα expression on MKs by flow cytometry. The GPIbα MFI was divided by FSC_A to normalize by MK size. The results of five independent experiments performed on two different CNT and GPIbα^{N103D} clones are shown as mean±SEM, Mann-Whitney test. **D.** Ploidy analysis of control (CNT) and GPIbα^{N103D} (CD41^{+}CD42^{+}) MKs. On the left: representative picture of flow cytometry analysis. On the right: the histograms showing mean ploidy as mean±SEM, unpaired t-test, n=4. **E.** Representative transmission electron microscopy pictures of mature control (CNT) an GPIbα^{N103D} MKs (scale bar: 2 μm). **F.** Representative immunofluorescence staining pictures of mature control (CNT) an GPIbα^{N103D} MKs: F-Actin (red), VWF (green), DAPI (nuclei, blue). Scale bar: 10 μm, z-stack middle frame is shown.

Supplemental Figure 4

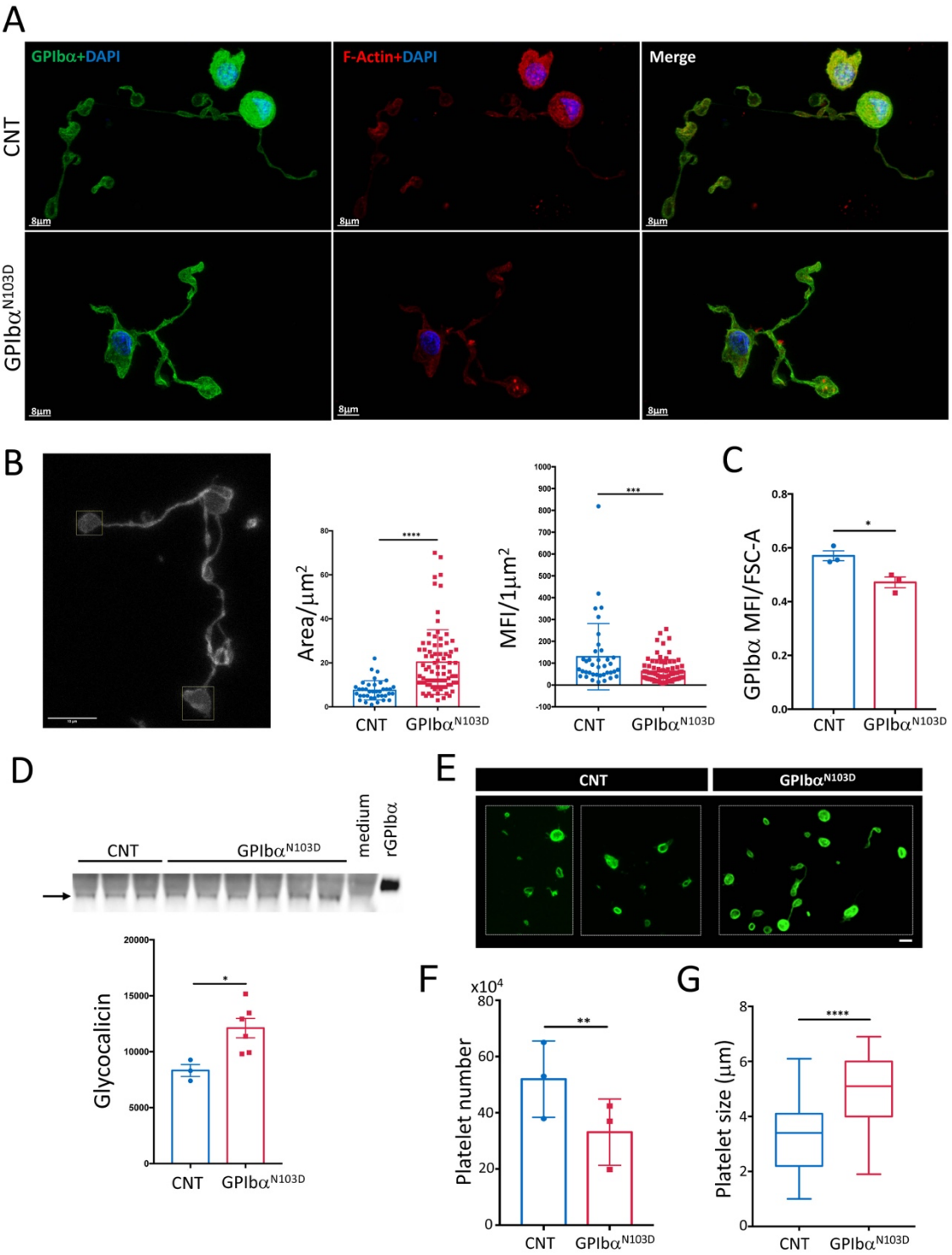

Supplemental Figure 4. GPIbα^{N103D} proplatelets display a slightly decreased GPIbα expression on tips as compared to controls. A. Representative immunofluorescence staining pictures of control (CNT) an GPIbα^{N103D} proplatelet forming MKs: CD42b (GPIbα, green), F-Actin (red), DAPI (nuclei, blue). Scale bar: 8µm, maximal projection is shown. **B.** Quantification of GPIbα expression. On the left: a representative picture of proplatelet forming-MK with squares depicting the areas of fluorescence measurement, z-stack middle frame is shown. On the right: the histograms presenting area (µm^2), and the Mean Fluorescence Intensity (MFI) of GPIbα, reported per 1µm2 as mean±SD, ***P<0.0005, unpaired t-test. At least 16

tips were analyzed for each of two control (CNT) and two GPIbα^{N103D} clones. **C.** Quantification of GPIbα expression on platelet-like particles generated *in vitro* by flow cytometry. The GPIbα MFI was divided by FSC_A to normalize by platelet size. The results of three independent experiments performed on three different CNT and GPIbα^{N103D} clones are shown as mean±SEM, **P*<0.01, Mann-Whitney test. **D.** Quantification of glycocalicin in culture media. Western blot analysis of glycocalicin in culture supernatants, rGPIb was used as a positive control[2] (increased size is due to a Tag) and medium without cells as negative control. The quantity of glycocalicin is expressed in arbitrary units as mean ± SEM (CNT: n=3, GPIbα^{N103D} n=6), **P*<0.05, unpaired t-test. **E-G.** Platelets recovered from the 3D silk bone marrow model functionalized with fibronectin (50 µg/mL). **E.** Representative picture of *ex vivo*-released control (CNT) and GPIbα^{N103D} platelets stained for β-tubulin (green). Scale bar: 5 µm, maximal projection is shown. **F.** The number of recovered platelets, data are expressed as mean ± SEM (CNT n=3, GPIba^{N103D} n=3), ***P*<0.01, unpaired t-test. **G.** Platelet diameters (µm) of *ex vivo*-released platelets measured by Arivis Vision 4D (Zeiss). Data are expressed as mean ± min to max, CNT: n=75, GPIbα^{N103D}: n=75, **P*<0.05, unpaired t-test.

Supplemental Figure 5

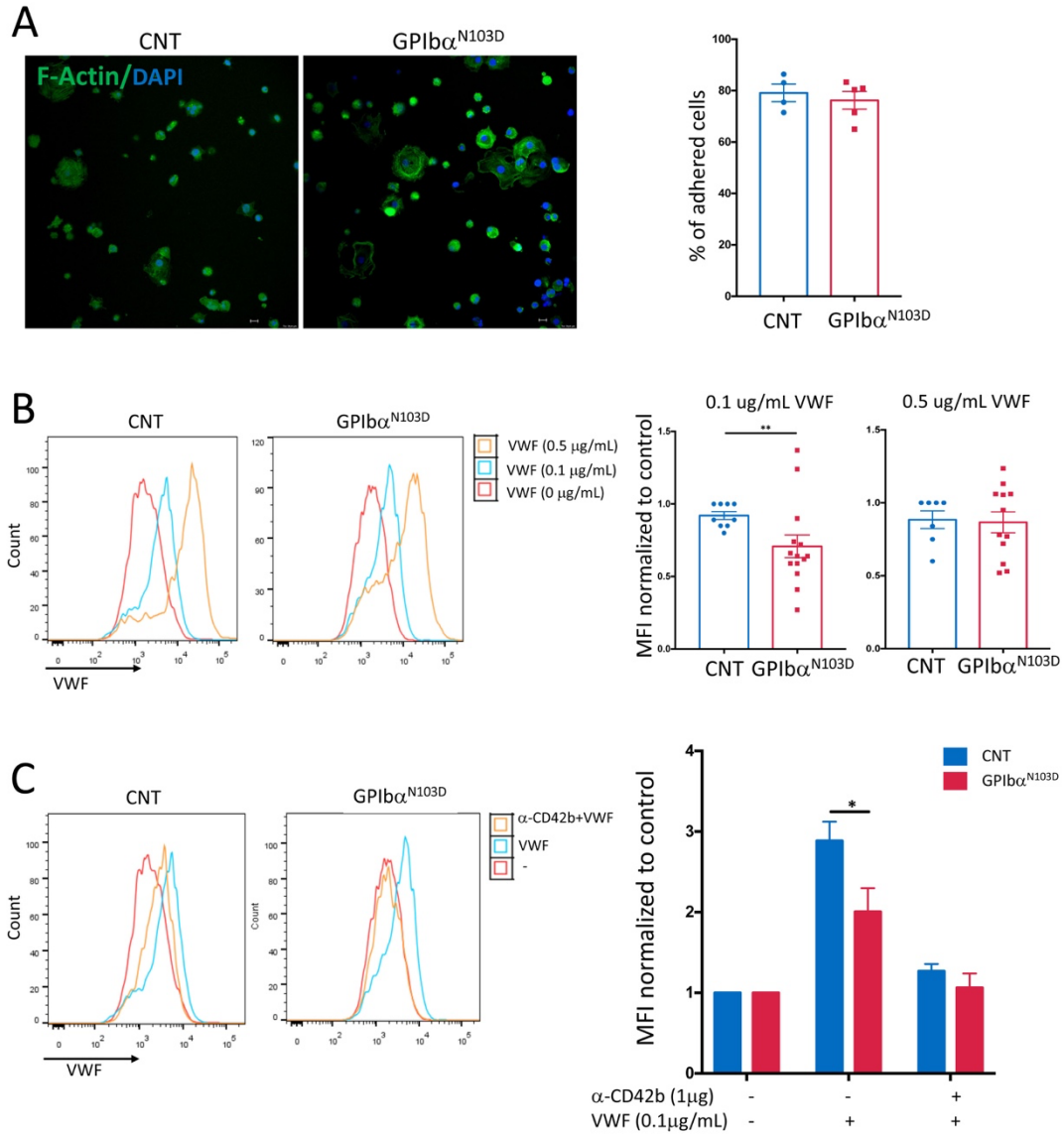

Supplemental Figure 5. Decreased VWF binding to GPIbα^{N103D} mutant. A. Mature control (CNT) and GPIbα^{N103D} Mks were adhered for 30 min on slides coated with 1µg/mL of VWF. Representative pictures of immunofluorescence staining of F-Actin (green) and DAPI (nuclei, blue) are shown on the left, single z-stack frame at the glass adhesion site is shown. The histogram on the right represents the percentage of adhered cell. Data are expressed as mean ± SEM (CNT n=4, GPIbα^{N103D} n=5). **B.** Flow cytometry analysis of ristocetin-induced VWF binding to mature control (CNT) and GPIbα^{N103D} MKs. Representative plots are shown on the left panel. Different concentrations of VWF were used as indicated. Mean fluorescence was normalized to one control (CNT) cell line in each experiment (on the right panel). Four independent experiments were done with at least two different CNT lines and three different GPIbα^{N103D} clones in each experiment. Data are expressed as mean ± SEM (CNT n=9, GPIbα^{N103D} n=14), $^{**}P<0.01$, Mann-Whitney test **C.** Representative pictures of flow cytometry plots showing the VWF binding on mature control (CNT) and GPIba^{N103D} MKs incubated with 1 ug of human anti-CD42b monoclonal antibody prior to incubation with ristocetin- and 0.1 µg/mL of VWF. Mean fluorescence intensity (MFI) was normalized to control cell lines (on the right panel). Data are expressed as mean ± SEM (CNT n=3-5, GPIbα^{N103D} n=3), $^{*}P<0.05$ unpaired t-test.

Supplemental Figure 6

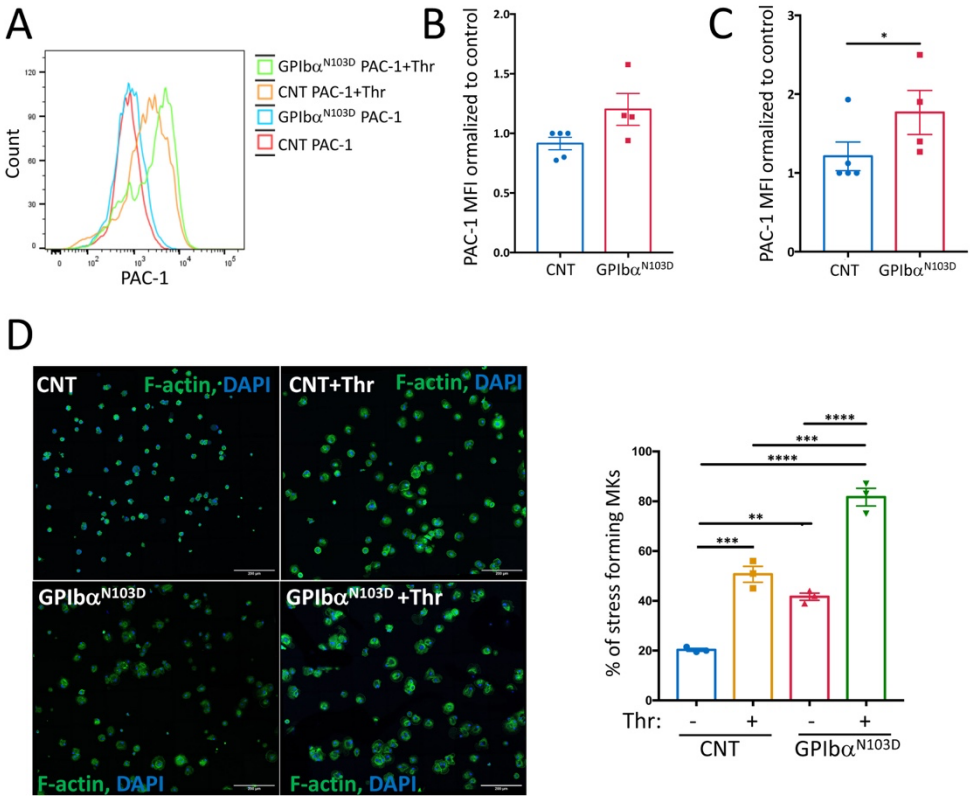

Supplemental Figure 6. Analysis of αIIbβ3 receptor activation. Flow cytometry analysis of PAC-1 binding to αIIbβ3 receptor on control (CNT) and GPIbα^{N103D} mutant MKs at basal state and after its activation by Thrombin (Thr). Monoclonal PAC-1-APC antibody that recognizes the fibrinogen binding site exposed on the activated form of the αIIbβ3 receptor was used. **A.** Representative picture of plots is shown on the left panel. **B-C.** The histograms present the mean fluorescence intensity (MFI) of PAC-1 normalized to 1 control in each experiment. Three independent experiments are shown. Data are expressed as mean ± SEM (CNT n=5, GPIba^{N103D} n=4). **P*<0.05, Mann-Whitney test. **B.** Basal state. **C.** MKs were stimulated for 5 minutes with Thrombin (1U/mL). **D.** Immunofluorescence analysis of stress fibers formation by mature control (CNT) and GPIbα^{N103D} mutant MKs stimulated with thrombin (Thr). Mature MKs were plated on fibrinogen-coated surface in the presence or absence of thrombin (1U/mL) for 30 min and stained for F-Actin (green) and DAPI (blue). Representative pictures of immunofluorescence staining are shown on the left panel. Scale bar: 200 µm, single z-stack frame at the glass adhesion site is shown. The histogram presenting the frequency (%) of stress fiber forming MKs plated on fibrinogen-coated surface in the presence or absence of thrombin is on the right panel. Data are expressed as mean ± SEM, n=4, ***P*<0.01, ****P*<0.005, *****P*<0.001. One Way Analysis of Variance (ANOVA) with Tukey's multiple comparison method was used.

Supplemental Figure 7

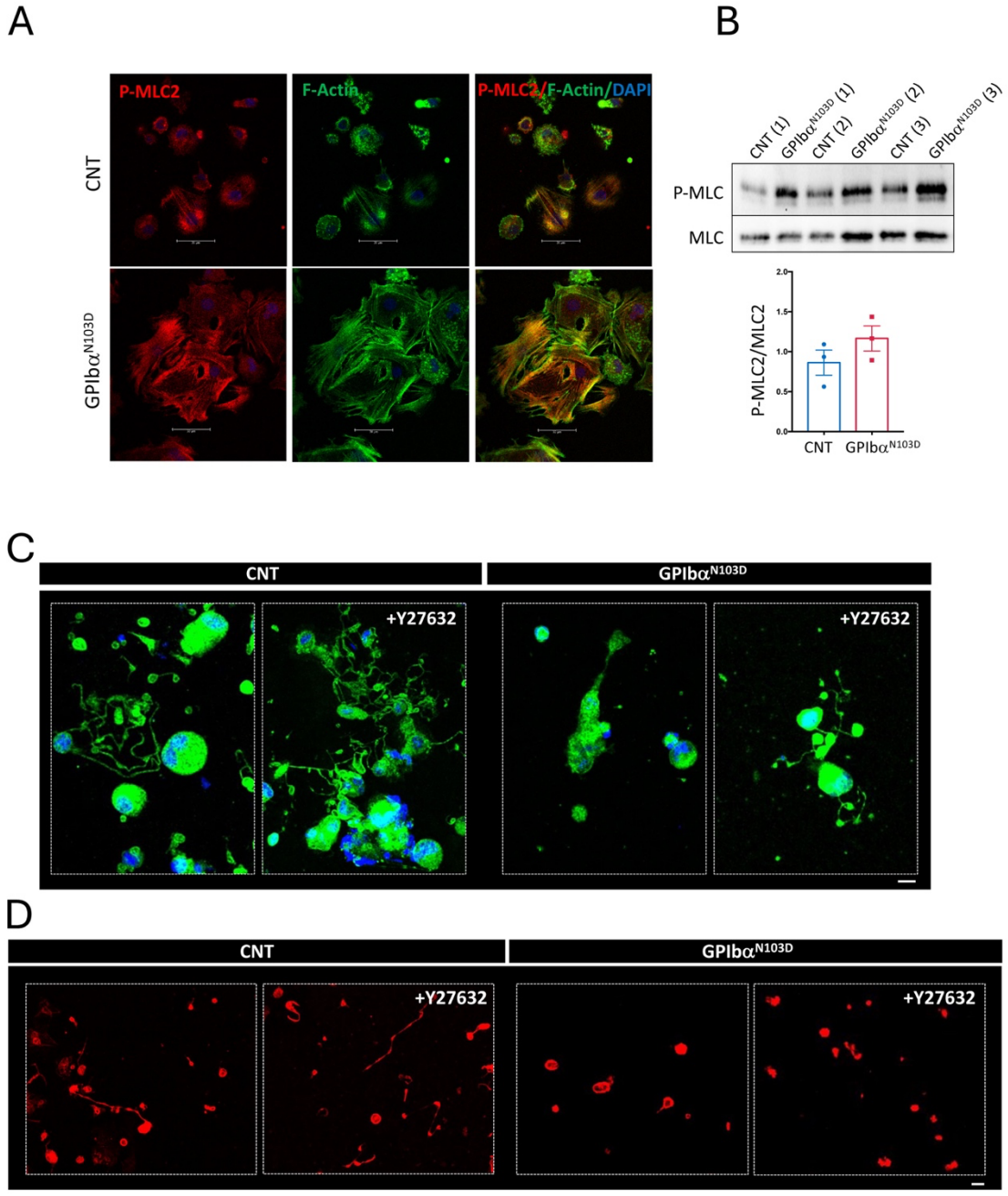

Supplemental Figure 7. GPIbα^{N103D} induces RhoA activation in megakaryocytes. A. Representative pictures of P-MLC2 (red), F-Actin (green) and DAPI (blue) staining of control (CNT) and GPIbα^{N103D} mutant MKs after adhesion on Fibrinogen, single z-stack frame at the glass adhesion site is shown. **B.** Western blot analysis of P-MLC2 in control (CNT) and GPIbα^{N103D} mutant MKs after 30 min incubation on fibrinogen-coated surface. Immunoblots were probed with Abs directed against P-MLC2, and MLC-2. Picture of immunoblot is shown on the top panel. Quantification of P-MLC2/total MLC2 is shown on the bottom panel. Data are expressed as mean±SEM, n=3. **C.** Immunofluorescence analysis of proplatelet formation by mature control (CNT) and GPIbα^{N103D} mutant MKs. Mature MKs were adhered on the fibrinogen-coated surface in the presence or absence of ROCK1/2 inhibitor Y27632, for 24 hours and stained for β-tubulin (green) and DAPI (blue). Scale bar: 10 µm, maximal projection is shown. **D.** Representative picture of *ex vivo*-released platelets with or without ROCK1/2 inhibitor Y27632 stained for β-tubulin (red). Scale bar: 5 µm, maximal projection is shown.

Supplemental Figure 8

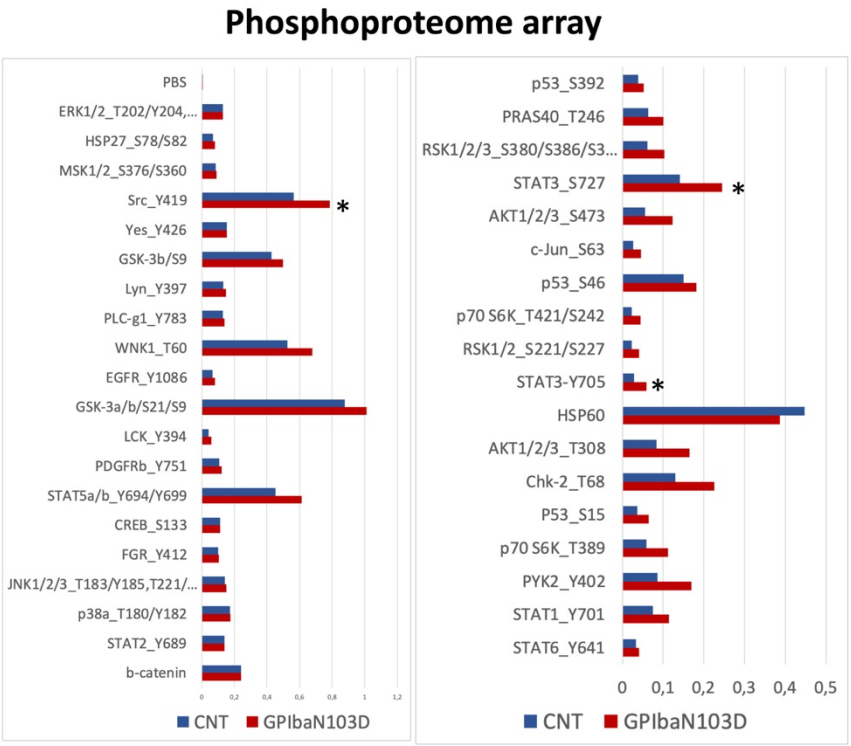

Supplemental Figure 8. Phosphoproteome analysis of control (CNT) and GPIbα^{N103D} mutant MKs. Mature MKs were seeded on fibrinogen-coated surface for 30 min, lysed and phospho-kinases were analyzed using membrane-based human phospho-kinase antibody array. The second experiment is shown.

Supplemental Figure 9

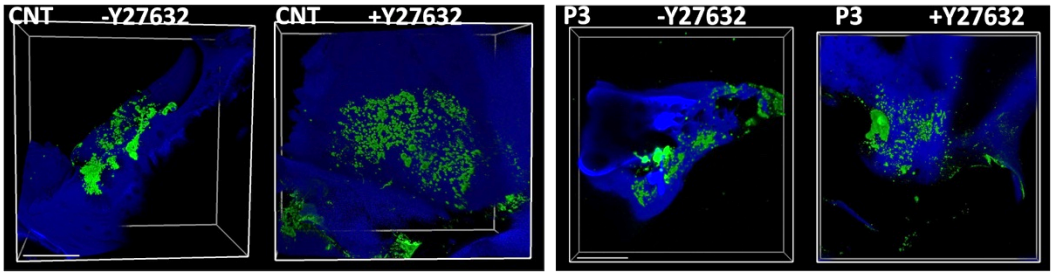

Supplemental Figure 9. RhoA inhibition restores platelet production from GPIbα^{N103D} megakaryocytes. MKs were seeded into the silk sponge with or without ROCK1/2 inhibitor Y27632. Representative picture of control and P3 proplatelet forming MKs. MKs and platelets are stained with anti-CD61 antibody (green) and silk sponge is in blue. Scale bar: 50 μm, full 3D volume is shown.

Supplemental Figure 10

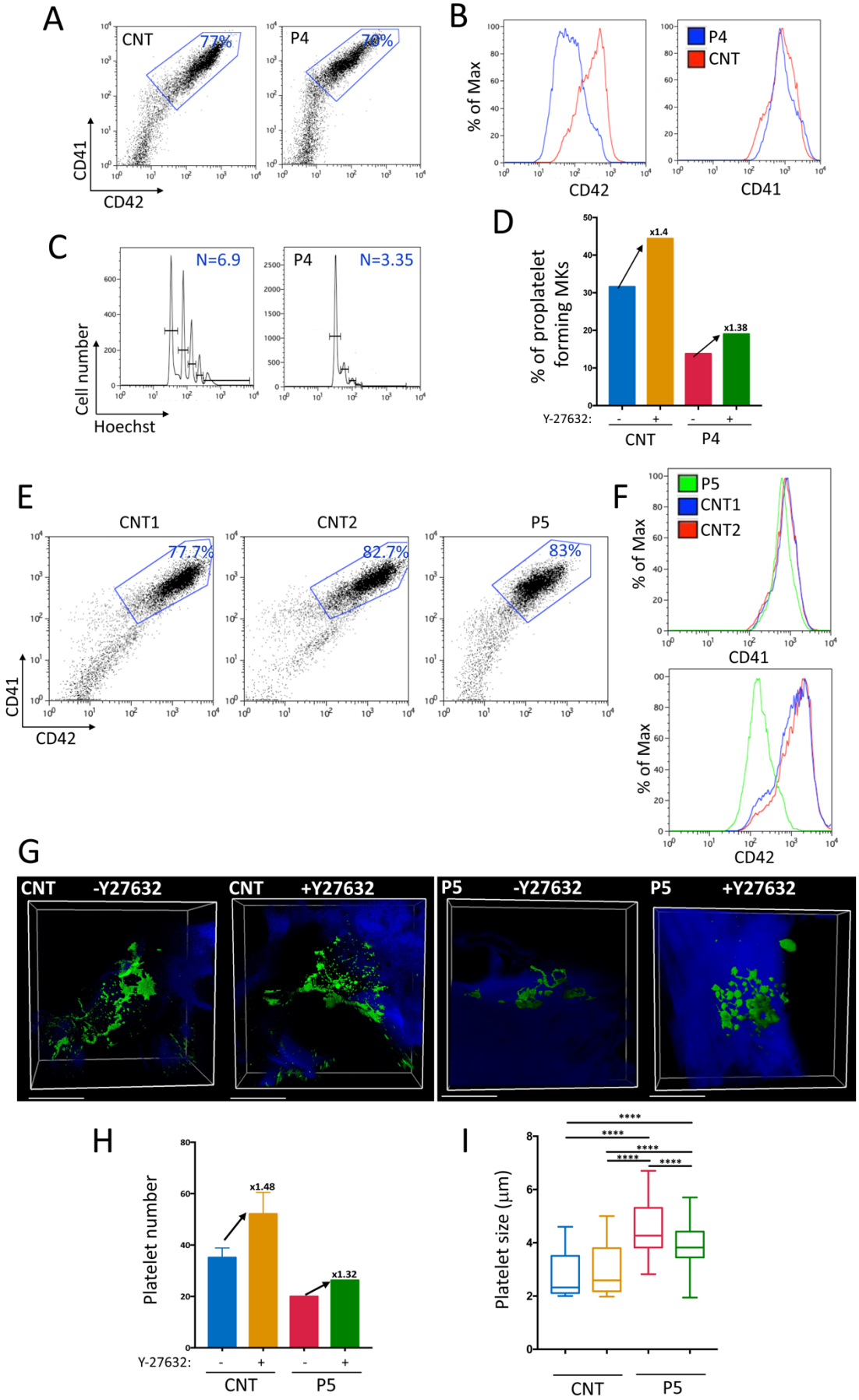

Supplemental Figure 10. RhoA inhibition does not affect platelet generation in homozygous BSS. Hematopoietic progenitors were isolated from peripheral blood of three healthy controls and two patients carrying homozygous *GP1BB* p.G43W (P4) and *GP1BA* p.L139P (P5) mutation respectively and cultured in presence of TPO and SCF for 10 days. **A-C.** Flow cytometry analysis of control (CNT) and patient 4 (P4) MKs. **A.** % of mature $CD41^+CD42^+$ MKs. **B.** CD41 and CD42 expression level. **C.** Ploidy level. $CD41^+CD42^+$ cells were incubated with Hoechst for 2h to label nucleus. N represents a mean ploidy level. **D.** Mature MKs were cultured on fibrinogen-coated surface in presence or absence of ROCK1/2 inhibitor Y27632 for 3 days. The histogram represents the frequency (%) of proplatelet forming MKs. A 1.4-fold increase was detected for control after incubation with ROCK1/2 inhibitor and 1.38-fold increase for P4 after incubation with ROCK1/2 inhibitor. **E-F.** Flow cytometry analysis of two control (CNT1, CNT2) and patient 5 (P5) MKs. **E.** % of mature $CD41^+CD42^+$ MKs. **F.** CD41 and CD42 expression level. **G-I.** MKs were seeded into the silk sponge with or without ROCK1/2 inhibitor Y27632. **G.** Representative picture of control and P5 proplatelet forming MKs. MKs and platelets are stained with anti-CD61 antibody (green) and silk sponge is in blue. Scale bar: 50 μm, maximal projection is shown. **H.** Silk scaffolds were perfused with culture media for 6 hours, and released platelets were collected into gas-permeable bags. Samples were mixed with counting beads to quantify the number of platelets that are identified as $CD41^+CD42a^+$ events. The number of recovered platelets is normalized to control (CNT). A 1.48-fold increase in platelet number was detected for controls after incubation with ROCK1/2 inhibitor (n=3, data are presented as mean±SD) and 1.32-fold increase for P5 after incubation with ROCK1/2 inhibitor. **I.** Platelet diameters (μm) of *ex vivo*-released platelets with or without ROCK1/2 inhibitor Y27632 were measured by Arivis Vision 4D (Zeiss). Data are expressed as mean ± min to max, CNT: n=83, CNT+Y27632: n=83, P3: n=83, P3+Y27632: n=89, ****P<0.0001, One Way Analysis of Variance (ANOVA) with Tukey's multiple comparison method was used.

Supplemental References

1. Latger-Cannard V, Philippe C, Bouquet A, et al. Haematological spectrum and genotype-phenotype correlations in nine unrelated families with RUNX1 mutations from the French network on inherited platelet disorders. *Orphanet J Rare Dis*. 2016;11:49.
2. Vanhoorelbeke K, Cauwenberghs N, Vauterin S, et al. A reliable and reproducible ELISA method to measure ristocetin cofactor activity of von Willebrand factor. *Thromb Haemost.* 2000;83(1):107-113.
3. Otsu, N. A threshold selection method from gray-level images. *IEEE Transactions on Systems, Man, and Cybernetics.* 1979; 9(1), 62-66.
4. Rockwood DN, Preda RC, Yücel T, Wang X, Lovett ML, Kaplan DL. Materials fabrication from Bombyx mori silk fibroin. *Nat Protoc*. 2011;6(10):1612-1631.
5. Di Buduo CA, Soprano PM, Tozzi L, et al. Modular flow chamber for engineering bone marrow architecture and function. *Biomaterials*. 2017;146:60-71.
6. Di Buduo CA, Laurent PA, Zaninetti C, et al. Miniaturized 3D bone marrow tissue model to assess response to Thrombopoietin-receptor agonists in patients. *Elife*. 2021;10.
7. Di Buduo CA, Wray LS, Tozzi L, et al. Programmable 3D silk bone marrow niche for platelet generation ex vivo and modeling of megakaryopoiesis pathologies. *Blood*. 2015;125(14):2254-2264.
8. Donada A, Balayn N, Sliwa D, et al. Disrupted filamin A/α(IIb)β(3) interaction induces macrothrombocytopenia by increasing RhoA activity. *Blood*. 2019;133(16):1778-1788.